Cell Reports

Article

4EHP and GIGYF1/2 Mediate Translation-Coupled Messenger RNA Decay

Graphical Abstract

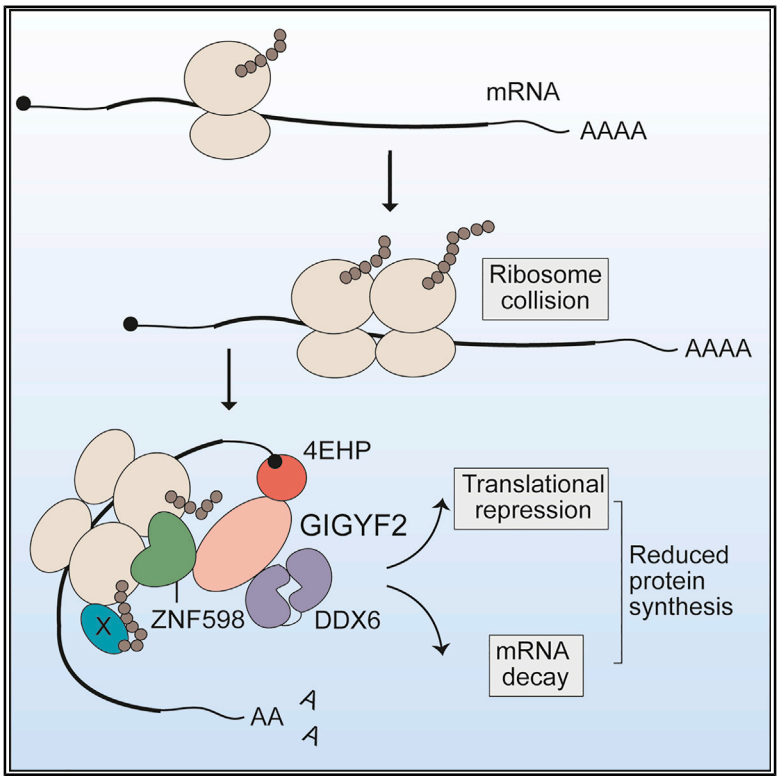

Highlights

- 4EHP and GIGYF1/2 induce co-translational mRNA decay
- Targeted transcripts are characterized by ribosome pausing and collision
- mRNA decay requires ribosome pausing, DDX6, and partially ZNF598
- Identified mRNAs encode secreted and membrane-bound proteins or tubulin subunits

Authors

Ramona Weber, Min-Yi Chung, Csilla Keskeny, ..., Eugene Valkov, Elisa Izaurralde, Cátia Igreja

Correspondence

catia.igreja@tuebingen.mpg.de

In Brief

The quality of the proteome is crucial for cell survival. Weber et al. show that the destruction of a subset of messages marked by altered ribosome activity is triggered by the 4EHP-GIGYF1/2 complexes during protein synthesis. This function of the complexes averts the production of unwanted or cytotoxic proteins.

Weber et al., 2020, Cell Reports *33*, 108262
October 13, 2020
https://doi.org/10.1016/j.celrep.2020.108262

CellPress

Cell Reports

CellPress
OPEN ACCESS

Article

4EHP and GIGYF1/2 Mediate Translation-Coupled Messenger RNA Decay

Ramona Weber,[1] Min-Yi Chung,[1] Csilla Keskeny,[1,4] Ulrike Zinnall,[2,3] Markus Landthaler,[2,3] Eugene Valkov,[1,5] Elisa Izaurralde,[1,6] and Cátia Igreja[1,7,*]

[1]Department of Biochemistry, Max Planck Institute for Developmental Biology, Max-Planck-Ring 5, D-72076 Tübingen, Germany
[2]Berlin Institute for Medical Systems Biology (BIMSB), Max Delbrück Center for Molecular Medicine in the Helmholtz Association (MDC), 10115 Berlin, Germany
[3]IRI Life Sciences, Institute für Biologie, Humboldt Universität zu Berlin, 10115 Berlin, Germany
[4]Present address: Experimental and Clinical Research Center (ECRC), Max Delbrück Center and Charité Berlin, 13125 Berlin, Germany
[5]Present address: Messenger RNA Regulation and Decay Section, RNA Biology Laboratory, Center for Cancer Research, National Cancer Institute, Frederick, MD 21702-1201, USA
[6]Deceased 30th April 2018
[7]Lead Contact
*Correspondence: catia.igreja@tuebingen.mpg.de
https://doi.org/10.1016/j.celrep.2020.108262

SUMMARY

Current models of mRNA turnover indicate that cytoplasmic degradation is coupled with translation. However, our understanding of the molecular events that coordinate ribosome transit with the mRNA decay machinery is still limited. Here, we show that 4EHP-GIGYF1/2 complexes trigger co-translational mRNA decay. Human cells lacking these proteins accumulate mRNAs with prominent ribosome pausing. They include, among others, transcripts encoding secretory and membrane-bound proteins or tubulin subunits. In addition, 4EHP-GIGYF1/2 complexes fail to reduce mRNA levels in the absence of ribosome stalling or upon disruption of their interaction with the cap structure, DDX6, and ZNF598. We further find that co-translational binding of GIGYF1/2 to the mRNA marks transcripts with perturbed elongation to decay. Our studies reveal how a repressor complex linked to neurological disorders minimizes the protein output of a subset of mRNAs.

INTRODUCTION

Regulation of protein synthesis throughout the translation cycle safeguards the production of an optimal proteome. Changes in ribosome dynamics during elongation are required to fine-tune co-translational protein folding and regulate mRNA stability (Hanson and Coller, 2018; Hu et al., 2009; Radhakrishnan and Green, 2016). Factors such as codon or nascent peptide composition, secondary structures, ribosome-associated factors, defective ribosomes, and damaged or improperly processed mRNAs influence ribosome movement on the open reading frame (ORF) (reviewed in Buskirk and Green, 2017; Joazeiro, 2017).

Codon optimality is a conserved evolutionary mechanism that affects mRNA stability in a translation-dependent manner (Hanson and Coller, 2018). mRNAs enriched in slow decoding (non-optimal) codons tend to be more unstable than those enriched in fast decoding (optimal) codons (Presnyak et al., 2015). In the unstable transcripts, the slow translating ribosomes are recognized by the RNA helicase DDX6 and the CCR4-NOT complex, which then trigger mRNA decay (Buschauer et al., 2020; Radhakrishnan et al., 2016).

Translation-coupled mechanisms also control mRNA stability in response to the accumulation of unwanted or potentially cytotoxic proteins. Tubulin mRNAs are decayed in response to excess depolymerized tubulin (Cleveland et al., 1981; Gasic et al., 2019; Gay et al., 1989; Pachter et al., 1987). Binding of tetratricopeptide protein 5 (TTC5) to an N-terminal motif of tubulin activates, by yet unidentified factors, the decay of the ribosome-bound mRNA (Lin et al., 2020). Similarly, quality-control checkpoints sense defects in protein targeting to the endoplasmic reticulum (ER) and initiate mRNA degradation. Failure in the interaction of the signal recognition particle (SRP) with the signal sequence of the nascent protein or the receptor at the ER membrane results in the recruitment of the decay machinery to the translating mRNA (Karamyshev et al., 2014; Lakshminarayan et al., 2020; Pinarbasi et al., 2018). The molecular details of co-translational decay of secretome-associated mRNAs remain unclear.

Damaged or improperly processed mRNAs are also co-translationally degraded. Disruption of elongation in faulty transcripts causes ribosome stalling and collision, decreases translation, and has the potential to induce proteotoxic stress (Simms et al., 2017a). Thus, cells evolved surveillance mechanisms that coordinate the degradation of the truncated protein products and ribosome rescue with mRNA degradation (reviewed in Brandman and Hegde, 2016; Joazeiro, 2019; Simms et al., 2017a). Recognition and ubiquitination of the collided ribosomes by the E3 ubiquitin ligase ZNF598 (Garzia et al., 2017; Ikeuchi et al., 2019; Juszkiewicz et al., 2018; Juszkiewicz and Hegde, 2017; Simms et al., 2017b; Sundaramoorthy et al., 2017) activates mRNA decay (D'Orazio et al., 2019).

ZNF598 binds to the Grb10-interacting GYF (glycine-tyrosine-phenylalanine) domain proteins 1 and 2 (GIGYF1/2) that form a translational repressor complex with the cap-binding eIF4E-homologous protein (4EHP) (Morita et al., 2012). The GYF domain of GIGYF1/2 binds to proteins containing Pro-Pro-Gly-Φ motifs (Φ, hydrophobic amino acid with the exception of tryptophan), such as ZNF598, tristetraprolin (TTP), or the microRNA (miRNA)-induced silencing-complex-associated TNRC6 proteins (Fu et al., 2016; Morita et al., 2012; Schopp et al., 2017). These interactions integrate the 4EHP-GIGYF1/2 complexes in miRNA-mediated gene silencing, regulate cytokine production, and control gene expression during embryonic development (Fu et al., 2016; Giovannone et al., 2009; Kryszke et al., 2016; Morita et al., 2012; Schopp et al., 2017; Tollenaere et al., 2019). Together with the CCR4-NOT deadenylase complex and DDX6, 4EHP and GIGYF1/2 repress translation initiation and elicit mRNA decay (Amaya Ramirez et al., 2018; Peter et al., 2019; Ruscica et al., 2019).

Despite the interaction with ZNF598, GIGYF1/2 and 4EHP have not been associated with translational surveillance. Using translatome and transcriptome analysis, we explored the role of 4EHP-GIGYF1/2 complexes in the regulation of translation and mRNA stability. Our results highlight a role for this repressor complex in co-translational degradation of mRNAs, of which many encode secreted and membrane-bound proteins. Together with DDX6 and GYF-domain binding proteins, 4EHP and GIGYF1/2 induce decay of mRNAs with disturbed elongation. Our studies indicate that 4EHP and GIGYF1/2 are part of the cellular machinery that selectively reduces the abundance of actively translating mRNAs to fine-tune protein synthesis.

RESULTS

4EHP-GIGYF1/2 Complexes Regulate the Abundance of mRNAs Encoding Secreted and Membrane-Bound Proteins

To identify mRNAs regulated by 4EHP and GIGYF1/2, we studied genome-wide translational changes by using ribosome profiling (Ingolia et al., 2009). Isolation and identification of ribosome-protected fragments coupled to transcriptome analysis were performed in control (Ctrl), CRISPR-Cas9-engineered GIGYF1/2 null (knockout [KO]) (Peter et al., 2017), and 4EHP null (Räsch et al., 2020) HEK293T cells (Figures S1A and S1B). The experiments were reproducible as ribosomal footprints (Ribo-seq) and RNA sequencing (RNA-seq) library replicates clustered together (Figures S1C and S1D).

To detect variations in translational efficiency (TE) across experimental conditions, genes were plotted according to changes in mRNA abundance and ribosome occupancy (Figures 1A and 1B). Only a small subset of mRNAs showed altered TE in the absence of 4EHP (n = 24) or GIGYF1/2 (n = 7) (Figures 1A, 1B, S1E, and S1F; Table S1). However, in comparison to Ctrl cells, 497 and 341 mRNAs exhibited increased abundance in 4EHP null and GIGYF1/2 null cells, respectively (Tables S2 and S3). A significant fraction of the mRNAs was commonly upregulated in both null cells (n = 82, p = $1.4459e^{-34}$; Figure 1C; Table S4). Although 571 and 569 mRNAs were downregulated in 4EHP null and GIGYF1/2 null cells, there was no significant overlap among the two datasets (n = 38, p = 0.1963; Figure S1G). Reduction of mRNA levels may be a consequence of indirect effects after the loss of these proteins.

As 4EHP and GIGYF1/2 are negative regulators of mRNA stability (Amaya Ramirez et al., 2018; Kryszke et al., 2016; Ruscica et al., 2019), we focused our analysis on transcripts upregulated in both cell lines (target mRNAs). GIGYF1/2 and 4EHP target mRNAs were overrepresented for genes encoding cell surface and extracellular proteins (Figures 1D and 1E). Approximately half of the target mRNAs code for ER, membrane, or secreted proteins (Figure 1F) that are translated at the ER (Hermesh and Jansen, 2013). Thus, these data suggest that 4EHP-GIGYF1/2 complexes regulate the abundance of a subset of secretome mRNAs.

GIGYF1/2 Regulate mRNA Stability

We next determined target mRNA decay rates after transcriptional arrest by actinomycin D by using northern blot or qRT-PCR. Decay kinetics in Ctrl and GIGYF1/2 null cells fitted to an exponential decay with a single component and $R^2 \geq 0.78$ (Figure 2). We found that *DBNDD2*, *CD109*, *ITPR3*, and *NPTX1* mRNAs were stabilized in the absence of GIGYF1/2, as the corresponding half-lives ($t_{1/2}$) mostly doubled in these cells (Figure 2). In contrast, *β-ACTIN*—a non-target—was degraded similarly in Ctrl and null cells (Figure 2F). Therefore, GIGYF1/2 proteins are regulators of mRNA stability, as observed in *Drosophila* and human HeLa cells mainly using reporter assays (Amaya Ramirez et al., 2018; Kryszke et al., 2016; Ruscica et al., 2019).

Multiple GIGYF1/2 Co-factors Are Required for mRNA Decay

To obtain insight into the molecular mechanism, we probed if the assembly of the 4EHP-GIGYF1/2-DDX6 complex (Figure S1H) was required for mRNA decay. We measured mRNA abundance in GIGYF1/2 null cells upon transient co-expression of 4EHP and wild-type (WT) or mutants of the GIGYF paralogs (Figures S1I and S1J). In GIGYF1/2 null cells, target levels increased more than 2-fold, but not *β-ACTIN* (Figures 3A, 3B, and S1K). mRNA decay was restored when 4EHP was co-expressed with GIGYF1/2, but not with the mutants unable to associate with 4EHP (C*), DDX6 (DDX6*), or PPGΦ-containing proteins (GYF domain mutant; GYF*) (Ash et al., 2010; Peter et al., 2017, 2019; Figures 3A, 3B, and S1K). Moreover, failure in the assembly of the full complex also compromised *DBNDD2* turnover (Figure S1L). Re-expression of GIGYF1/2 alone was not sufficient to induce mRNA decay in the null cells (data not shown), as 4EHP and GIGYF1/2 protein stabilities are co-regulated (Figures S1A and S1B; Morita et al., 2012).

Likewise, the levels of *NPTX1*, *CD109*, and *ITPR3* in 4EHP null cells were also at least 2-fold higher (Figure S2A). Target mRNA decay was restored upon co-expression of the 4EHP-GIGYF1/2 complex but not when 4EHP is unable to bind to the cap (cap*) and GIGYF1/2 (S*) (Peter et al., 2017). WT and mutant GIGYF1/2 or 4EHP expression levels were similar and did not affect the abundance of *β-ACTIN* (Figures 3B, S1K, S2A, and S2B).

These results indicate that 4EHP, DDX6, and GYF domain-associated protein(s) bind to GIGYF1/2 to promote target mRNA degradation.

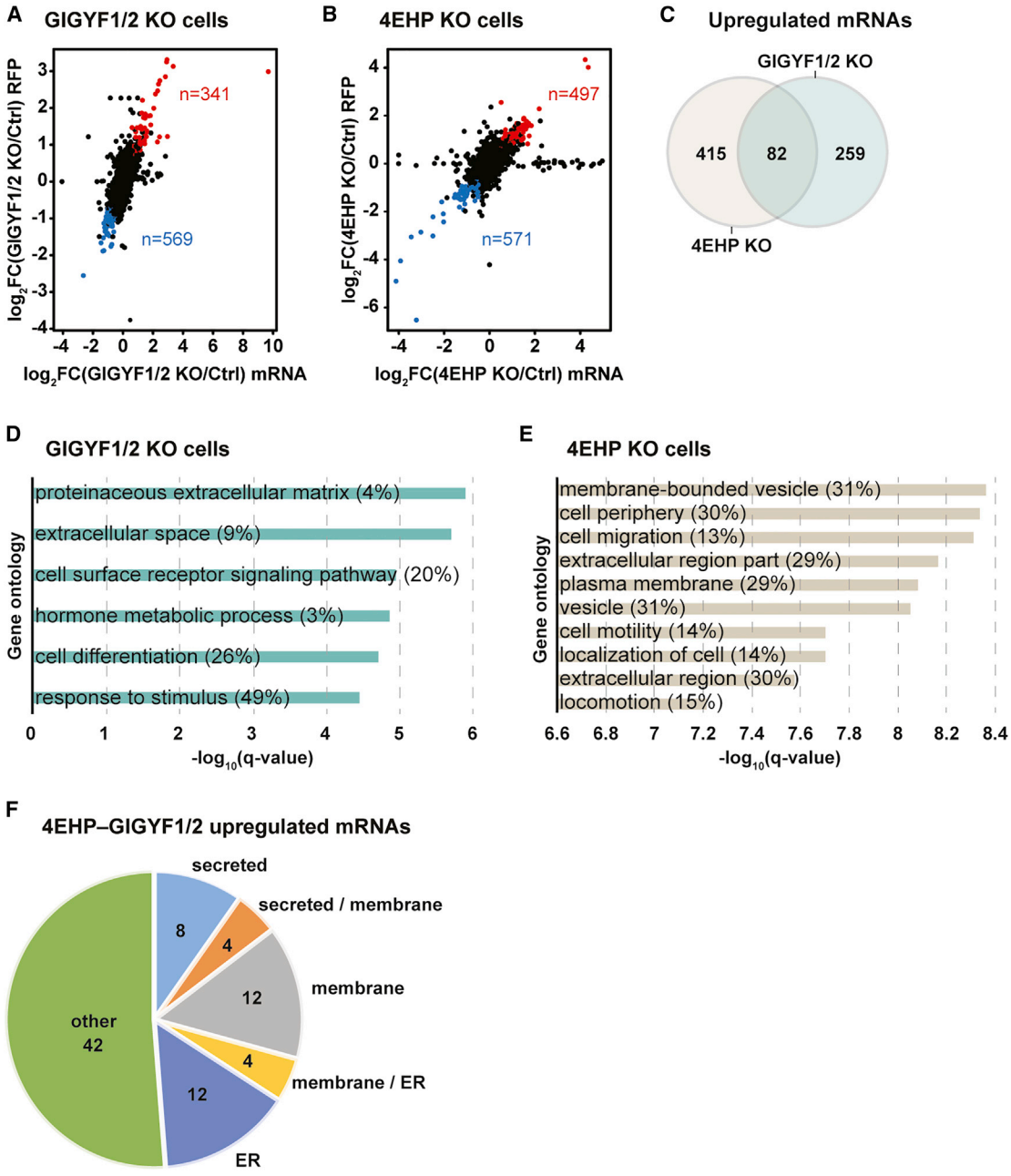

Figure 1. The 4EHP-GIGYF1/2 Complexes Regulate mRNA Abundance

(A and B) Genome-wide analysis of changes in ribosome footprints (RFPs) and mRNA abundance in GIGYF1/2 null (KO) and 4EHP null cells relative to control (Ctrl) cells. Logarithmic fold change in RFP (log_2FC) on the vertical axis is plotted as a scatter graph against the log_2FC of mRNA abundance. Each dot represents an individual gene (n = 9,870). Red, upregulated; blue, downregulated.

(C) Venn diagram showing the number of common and unique upregulated genes in 4EHP and GIGYF1/2 KO cells (n = 82; p = $1.4459e^{-34}$).

(D and E) Gene Ontology terms enriched in 4EHP-GIGYF1/2 target mRNAs. Bar graphs show $-log_{10}$ *q* values for each of the overrepresented category. Values in parentheses indicate the % of genes within each category.

(F) Number of 4EHP-GIGYF1/2 target mRNAs encoding endoplasmic reticulum (ER), membrane, or secreted proteins. See also Figure S1.

The GYF Domain of GIGYF2 Mediates mRNA Binding

To investigate the recruitment of the complex to target mRNAs, we performed RNA-immunoprecipitation (RNA-IP) assays and qRT-PCR. In contrast to GFP-MBP, GFP-GIGYF2 efficiently associated with *NPTX1*, *CD109*, *DBNDD2*, and *ITPR3* (Figures 3C–3F; IP graphs). GIGYF2 binding increased with the length of the target coding sequence (CDS), as longer sequences (*CD109* and *ITPR3*) showed higher binding efficiencies than

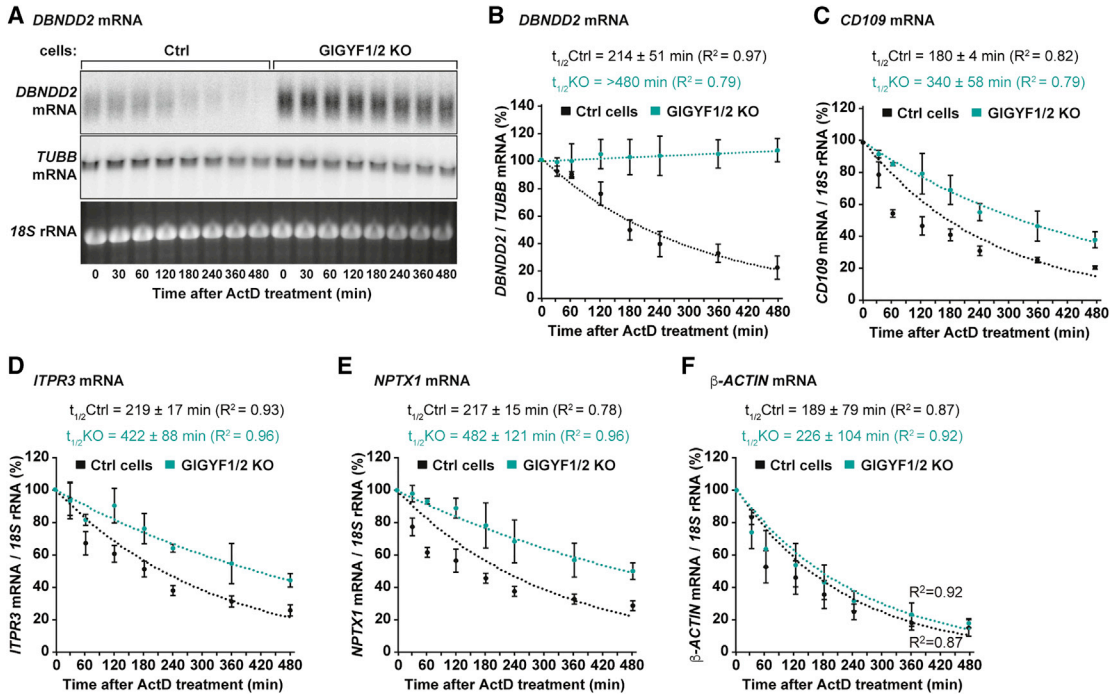

Figure 2. GIGYF1/2 Induce mRNA Decay

(A–F) Ctrl and GIGYF1/2 KO cells were treated with actinomycin D (ActD) and harvested at the indicated time points. RNA samples were analyzed by northern blotting (A and B) or qRT-PCR (C–F) and normalized to that of *TUBB* or *18S* rRNA. The value at time zero (before ActD addition) was defined as 100%. Results were plotted as a function of time. Circles represent the mean value and error bars the standard deviation (SD) (n = 3). The decay curves were fitted to an exponential decay with a single component (dotted lines). R^2 values are indicated for each curve. The half-life of each mRNA in Ctrl and KO cells is represented as the mean ± SD. *18S* rRNA; ethidium bromide staining shows equal loading.

shorter ones (*NPTX1* and *DBNDD2*). The interaction of GIGYF2 C* and DDX6* mutants with the different transcripts was comparable to WT protein. However, the association of the GIGYF2 GYF* mutant with mRNA was strongly reduced (Figures 3C–3F; IP graphs) indicating that target recognition relies on the GYF domain of GIGYF2. All proteins were expressed at equivalent levels and did not alter mRNA steady-state levels (Figures 3C–3F, input graphs, and 3G).

Similarly, V5-SBP-4EHP bound to target mRNAs in the presence of GIGYF2 WT or DDX6*, but not MBP, GIGYF2 C*, or GYF* (Figures S2C–S2E, pull-down graphs, and S2F). mRNA degradation, inferred from the steady-state mRNA levels, only occurred in cells co-expressing GIGYF2 WT (Figures S2C–S2E, input graphs). Our results indicate that binding of 4EHP to the mRNA cap requires GIGYF2 and that recruitment of the complex to the target mRNA is provided by proteins interacting with its GYF domain.

4EHP-GIGYF1/2 Complexes Trigger Co-translational mRNA Decay

Next, we dissected the mRNA features required for turnover. We generated reporters containing the CDS or the 3′ UTR of *DBNDD2* and *LGALS3BP* to express in cells. To measure protein levels, a hemagglutinin (HA) tag was inserted in frame with each CDS (Figure 4A), whereas the 3′ UTRs were preceded by *Renilla* luciferase ORF (R-LUC; Figure S2G).

DBNDD2-HA and LGALS3BP-HA protein levels were increased in GIGYF1/2 null cells (Figures 4B–4D). The corresponding transcripts were also more stable in the absence of GIGYF1/2 (Figures 4E, 4F, 4I, and 4J), indicating that the CDS is sufficient to recapitulate mRNA decay. In contrast, R-LUC activity and mRNA levels of the 3′ UTR reporters were similar in Ctrl and null cells (Figures S2H–S2J). Thus, target mRNA decay is independent of the 3′ UTR-associated mechanisms previously associated with the 4EHP-GIGYF1/2 complexes (Fu et al., 2016; Kryszke et al., 2016; Schopp et al., 2017; Tollenaere et al., 2019).

The observation that the CDS determined GIGYF1/2-dependent mRNA decay suggested that turnover occurred co-translationally. We examined the decay rate of intron-less CDS reporters containing a premature STOP three codons downstream of the AUG to prevent the synthesis of an HA-tagged protein (Figures 4A–4C). Interestingly, *DBNDD2-STOP$_3$-HA* and *LGALS3BP-STOP$_3$-HA* transcripts degraded with similar rates in Ctrl and null cells (Figures 4G–4J). Hence, GIGYF1/2-mediated mRNA decay requires translation of the CDS.

We then analyzed the association of GIGYF2 and targets with ribosomes by using sucrose density gradient separation (Figure S3A). GIGYF2 and its co-factor ZNF598 were mostly observed in the top fractions of the gradient corresponding to free ribonucleoprotein particles (RNPs) and 40S ribosome subunit (Figure S3A, lanes 1–6). However, both proteins were also

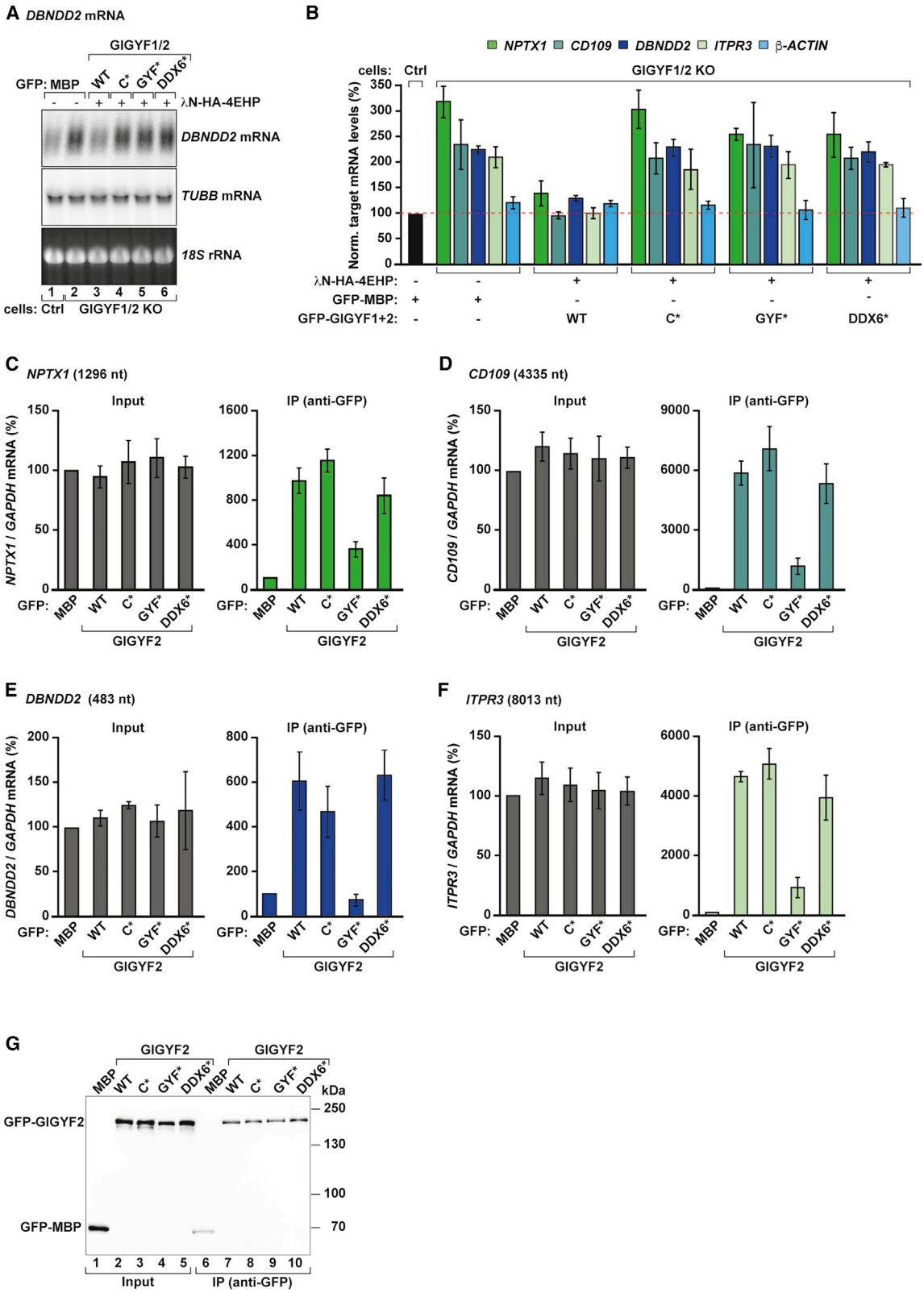

(legend on next page)

found in the heavy fractions of the gradient, as part of the signal was detected in polysomes (Figure S3A, lanes 13–16). In addition, GIGYF2 WT and GYF* mutant co-purified with the ribosomal protein eL22L1 (Figure S3B). Consistent with the idea of ribosome-associated decay, *DBNDD2*, *CD109*, *ITPR3*, and *NPTX1* were engaged in translation, as the majority of each mRNA was associated with polysomes or 80S monosomes (Figures S3C–S3F).

We also measured the interaction of GIGYF2 with mRNA in the absence of translation. Inhibition of translation with harringtonine or puromycin did not alter GIGYF2 expression but profoundly reduced its binding to *ENO2* (Figures S3G–S3J). *ENO2* is another bona fide target transcript as decay in null cells is restored upon re-expression of the 4EHP–GIGYF2 complex (Figure S3K).

Altogether, these results suggest that GIGYF2 associates with ribosomes to induce decay of actively translating mRNAs.

Ribosome Pausing Is Evident in 4EHP and GIGYF1/2 Target mRNAs

To further investigate the details of co-translational decay by 4EHP and GIGYF1/2, we had a closer look at the ribosome footprint distribution along the CDS of the regulated transcripts. We found pronounced pauses, characterized by the accumulation of unique ribosome footprints greater than the median footprint coverage of the gene, in several of the 4EHP and GIGYF1/2 targets (Figures 5A and S4; Table S4). There was no preference for location or peptide motif at the pause sites but several contained Proline (Pro) and negatively charged amino acids. Pro and acidic residues promote slow peptide bond formation and are enriched at ribosome pause sites (Pavlov et al., 2009; Pelechano and Alepuz, 2017; Schuller et al., 2017; Wohlgemuth et al., 2008).

In *LARGE2*, translation was stalled at a Pro-Pro-Asp (P_{57}, P_{58}, D_{59}) motif located in the N-terminal region of the protein (Figure S4A), a previously described strong pause site (Ingolia et al., 2011; Schuller et al., 2017). *LARGE2* has four predicted isoforms with distinct N-terminal regions. With the exception of the canonical version, all other LARGE2 isoforms lack the PPD motif due to large N-terminal truncations or a 30-amino-acid deletion that removes residues 30 to 59.

The translational pause present in *CXCL16* at a Pro-Gly-Asn (P_{45}, G_{46}, N_{47}) motif is located after a stretch of 10 hydrophobic residues, of which 9 are Leu (Figures S4B and S4C). It contains the PG dipeptide that is overrepresented in ribosome stall sequences in bacteria, yeast, and humans (Doerfel et al., 2013; Manjunath et al., 2019; Pelechano and Alepuz, 2017; Schuller et al., 2017).

Prominent examples of translation pauses were also observed in the *NCKIPSD*, *ENO2*, *IFRD2*, and *DBNDD2* (Figures 5A and S4D–S4F). Interestingly, several of the paused ribosomes were also identified in ribosome run off assays, coupled with ribosome profiling, performed in HEK293 cells treated with translational inhibitors (Lee et al., 2012). In *ENO2*, increased footprints were observed at two AUG codons (M_1 and M_{165}) following treatment with lactimidomycin (LTM). M_{165} marks the position of the ribosome pause observed in our profiling experiment. LTM associates with ribosomes with an empty E-site (Garreau de Loubresse et al., 2014), a feature of initiating ribosomes or elongating ribosomes with impaired decoding kinetics or slow peptide bond formation (Buschauer et al., 2020; Schmidt et al., 2016). As no alternative start sites or N-terminally truncated protein isoforms have been described for *ENO2*, the LTM footprint at M_{165} most likely represents a ribosome paused during elongation.

The ribosome stall observed at the Asp-Asp-Glu motif of *IFRD2* (D_{97}, D_{98}, E_{99}; Figure S4F) was still present after ribosome run off assays in harringtonine-treated cells. Harringtonine is an A-site inhibitor (Garreau de Loubresse et al., 2014) that predominantly marks ribosomes positioned at the start codon (Ingolia et al., 2011). The footprint in the presence of harringtonine at the DDE motif is not a translation start site. Thus, the associated ribosome did not conclude elongation (run off) following treatment with the drug. Furthermore, monosome and disome profiling in embryonic stem cells (Tuck et al., 2020) identified in the mouse *Ifrd2* mRNA increased disome occupancy at an equivalent position of the human transcript (Figure S4G). As disomes are a sign of ribosome collision and delayed elongation, these data confirm that stalled ribosomes accumulate at the DDE motif of *IFRD2*.

The translational stall detected in *DBNDD2* at the Phe-Glu-Asp (F_{23}, E_{24}, D_{25}) peptide was also observed at an equivalent position of the transcript after ribosome run off assays (Figure 5A). Again, the observed footprint most likely identifies a ribosome trapped during elongation because the underlying sequence is incompatible with a translation start site.

These findings indicate that 4EHP and GIGYF1/2 regulate mRNAs with perturbed translation elongation.

4EHP-GIGYF1/2-Dependent Decay Partially Relies on ZNF598

The presence of ribosome stalling and collision in GIGYF1/2-regulated transcripts suggests that decay is coupled to translation surveillance and ZNF598. We applied RNA-seq and Ribo-seq to *ZNF598* null cells (Figures S5A–S5C). In these cells, the main changes occurred at the mRNA level, as only a minor fraction of genes (n = 7; Table S1) displayed significant changes in TE (Figures S5D and S5E). From the group of genes with increased

Figure 3. GIGYF1/2 Recruit Multiple Effector Proteins to Induce mRNA Decay

(A and B) Ctrl and GIGYF1/2 KO cells were transfected with λN-HA or λN-HA-4EHP, GFP-MBP, and GFP-GIGYF1/2 (WT or mutants). *DBNDD2* mRNA levels were determined by northern blotting, normalized (Norm.) to *TUBB*, and set to 100% in Ctrl cells. *NPTX1*, *CD109*, *ITPR3*, and *β-ACTIN* mRNA levels were quantified by qRT-PCR and normalized to those of *18S* rRNA. Bars represent the mean value and error bars the SD (n = 3). GIGYF1/2 mutants are as follows: C* (4EHP-binding mutant), GYF* (GYF domain mutant), and DDX6* (DDX6-binding mutant).

(C–F) GFP immunoprecipitation (IP) assays were performed in cells transfected with GFP-MBP or GFP-GIGYF2 (WT or mutants). mRNA levels in input (0.8%) and IP samples (12%) were quantified by qRT-PCR, normalized over *GAPDH*, and set to 100% in the presence of MBP. Bars indicate the mean value and error bars the SD (n = 3). The length of the CDS of each mRNA is indicated in nucleotides (nt).

(G) Immunoblot depicting the expression of the immunoprecipitated proteins. Inputs and immunoprecipitates were 2% and 2.7%, respectively. See also Figure S2.

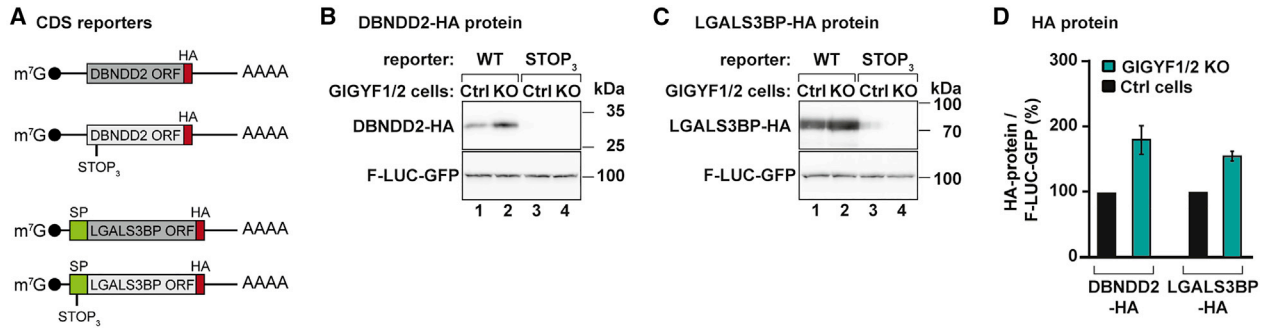

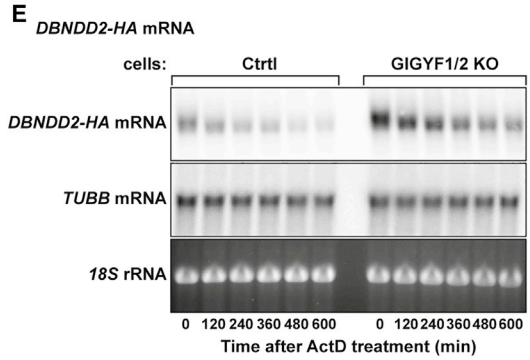

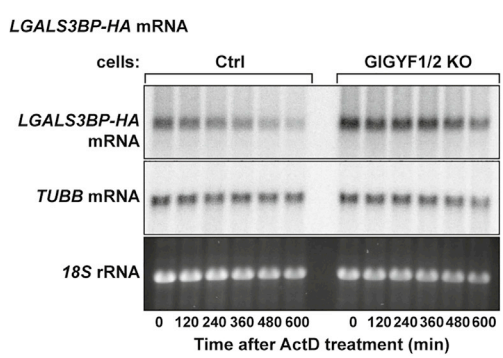

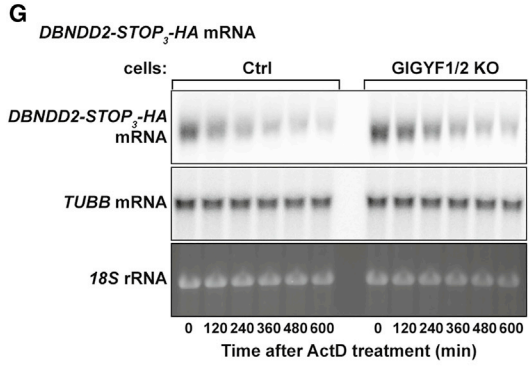

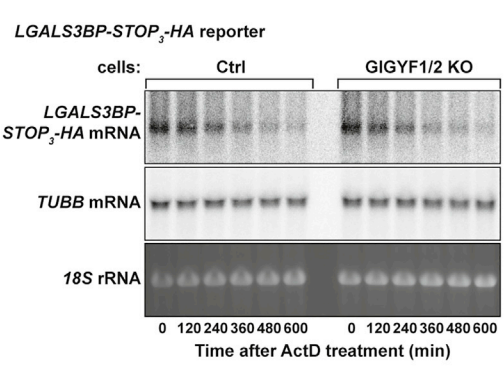

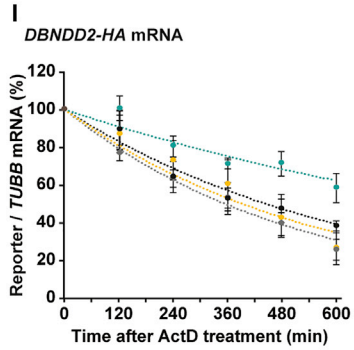

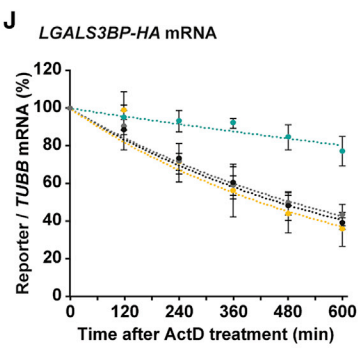

- Ctrl cells + *DBNDD2-HA* $t_{1/2}$ = 451 ± 67 min (R^2 = 0.97)
- Ctrl cells + *DBNDD2-STOP$_3$-HA* $t_{1/2}$ = 358 ± 48 min (R^2 = 0.99)
- GIGYF1/2 KO + *DBNDD2-HA* $t_{1/2}$ > 600 min (R^2 = 0.91)
- GIGYF1/2 KO + *DBNDD2-STOP$_3$-HA* $t_{1/2}$ = 404± 105 min (R^2 = 0.95)

- Ctrl cells + *LGALS3BP-HA* $t_{1/2}$ = 460 ± 27 min (R^2 = 0.99)
- Ctrl cells + *LGALS3BP-STOP$_3$-HA* $t_{1/2}$ = 491 ± 52 min (R^2 = 0.99)
- GIGYF1/2 KO + *LGALS3BP-HA* $t_{1/2}$ > 600 min (R^2 = 0.90)
- GIGYF1/2 KO + *LGALS3BP-STOP$_3$-HA* $t_{1/2}$ = 418 ± 36 min (R^2 = 0.96)

(legend on next page)

mRNA abundance in the null cells (n = 357), 9.2% and 14% were also upregulated in the absence of GIGYF1/2 ($p = 3.089792e^{-8}$) or 4EHP ($p = 2.37387e^{-12}$), respectively (Figure S5F; Table S6). 4EHP, GIGYF1/2, and ZNF598 commonly upregulated transcripts (n = 6), included *ENO2* and *CXCL16*, which display prominent ribosome pauses (Figures S4B and S4E). Increased transcript levels were the result of enhanced mRNA stability as the $t_{1/2}$ of *ENO2* and *CXCL16* increased in the absence of ZNF598 (Figures S5G and S5H). Thus, co-translational decay of a subset of 4EHP and GIGYF1/2 targets is dependent on ZNF598.

Ribosome Pausing Initiates 4EHP-GIGYF1/2-Dependent mRNA Decay

To confirm that ribosome pausing in GIGYF1/2 and 4EHP targets induces mRNA decay, we investigated the significance of the translational stall present in *DBNDD2*. We introduced a premature STOP before the pause site in the *DBNDD2-HA* reporter ($STOP_{18}$; Figure 5B) and measured mRNA levels in cells. Consistent with a failure to degrade mRNA in the absence of the translational pause, *DBNDD2-STOP$_{18}$-HA* levels did not vary in cells lacking GIGYF1/2 (Figures 5C and 5D).

DBNDD2 is a Pro-rich protein with two Pro tripeptides (P_{46}, P_{47}, P_{48} and P_{85}, P_{86}, P_{87}). Although we have not observed ribosome stalling at these positions, poly-Pro motifs are known to interfere with elongation (Gardin et al., 2014; Gutierrez et al., 2013; Ingolia et al., 2011; Pavlov et al., 2009; Wohlgemuth et al., 2008). We generated reporters with STOPs that prevented ($STOP_{39}$ and $STOP_{79}$) or allowed ($STOP_{89}$) the translation of the poly-Pro sequences by the ribosome (Figure 5B). As observed for WT *DBNDD2-HA*, the abundance of the reporters with STOPs after the FED motif was regulated by the 4EHP-GIGYF2 complex (Figures 5B–5D). Thus, only the identified ribosome pause is required for GIGYF1/2-dependent degradation of the *DBNDD2-HA* mRNA. All the premature STOPs blocked the synthesis of HA-tagged proteins (Figure 5C) and did not significantly alter the expression of the different reporters (Figure S6A). Because the degradation efficiency of nonsense-mediated decay (NMD) substrates in HEK293 cells is low (Gerbracht et al., 2017), the abundance of *DBNDD2-STOP$_{18}$-HA* was unaltered in UPF1-depleted cells (Figures S6B and S6C).

To test if impaired decoding or slow peptide bond formation at the pause site results in destabilization of *DBNDD2*, we substituted the FED motif by triple alanine (Figure 5B). However, the levels of the DBNDD2-FED_{25}-AAA-HA protein still responded to variations in GIGYF1/2 levels (Figure S6D). These data indicate that although the ribosome is paused at the FED motif (Figure 5A), translational pausing and subsequent mRNA turnover must be caused by another mechanism. As in the case of tubulin autoregulation (Lin et al., 2020), we explored the possibility that mRNA stability was controlled by factors that recognize the nascent chain and interfere with elongation. We altered the N terminus of DBNDD2 (M_1AAA instead of M_1DPN) and assessed reporter mRNA and protein levels. In Ctrl cells, *DBNDD2-DPN$_4$-AAA-HA* mRNA was better expressed and more stable than the WT reporter (Figures 5E and 5F). Moreover, its protein levels were not regulated by GIGYF1/2 (Figure S6D). These results show that the first translated codons of *DBNDD2-HA* are required for decay in a GIGYF1/2-dependent manner. One plausible explanation is that factors binding to the emergent nascent chain modulate ribosome occupancy, cause ribosome pausing, and promote GIGYF1/2-dependent destabilization of the transcript. In this scenario, the ribosome pauses at a location in the mRNA reflecting the distance traveled by the nascent chain inside the ribosome tunnel.

GIGYF1/2-Dependent mRNA Decay Can Occur during Co-translational ER Targeting

Many of the 4EHP-GIGYF1/2 target mRNAs encode signal peptide (SP)-containing proteins (Figure 1F) that undergo SRP-dependent translocation to the ER. Binding of SRP to the SP transiently interferes with translation elongation and leads to stacking and ribosome collision at the 5′ end of the CDS (Arpat et al., 2020; Walter and Blobel, 1981; Wolin and Walter, 1988, 1989).

To study if translational pausing associated with ER targeting is linked to GIGYF1/2-mediated mRNA decay, we made use of the *LGALS3BP-HA* reporter. LGALS3BP is a secreted protein containing a SP with 18 amino acids in length. Consistent with translational pausing during targeting to the ER, ribosome footprints are detected downstream of the signal sequence (Asp_{21}) in run off assays performed in cells treated with harringtonine and LTM (Lee et al., 2012). Likewise, a disome peak is observed at Val_{60} (Han et al., 2020; Figure 6A).

We introduced STOP codons 30 and 60 residues after the initiating AUG to prevent (*STOP$_{30}$*) or allow (*STOP$_{60}$*) the exposure of the SP from the ribosome tunnel and the targeting of the mRNA to the ER (Figure 6B; Jan et al., 2014; Kowarik et al., 2002). The premature STOPs did not reduce transcript expression (Figure S6E) or trigger NMD, as *LGALS3BP-STOP$_{30}$-HA* mRNA levels remain the same in the presence (scramble short hairpin RNA [shRNA]) or absence of UPF1 (UPF1 shRNA; Figure S6F).

We observed that *LGALS3BP-HA* and *LGALS3BP-STOP$_{60}$-HA* mRNA levels increased in the absence of GIGYF1/2 and decreased upon re-expression of 4EHP and GIGYF2 (Figures 6C and 6D). In contrast, *LGALS3BP-STOP$_{30}$-HA* was more abundant in Ctrl cells, and its levels did not respond to changes in GIGYF1/2 expression (Figures 6C, 6D, and S6E). Our results indicate that GIGYF1/2-dependent mRNA decay requires the

Figure 4. GIGYF1/2 Mediates Co-translational mRNA Decay

(A) Schematic representation of the *DBNDD2-HA* and *LGALS3BP-HA* CDS reporters. ORF, open reading frame; HA, hemagglutinin; $STOP_3$, STOP positioned three codons downstream of AUG; SP, signal peptide.

(B–D) Ctrl and GIGYF1/2 KO cells were transfected with *DBNDD2-HA* or *LGALS3BP-HA* (WT or $STOP_3$) and *F-LUC-GFP*. Protein samples were analyzed by western blotting using anti-HA and anti-GFP antibodies. (D) DBNDD2-HA protein levels were quantified, normalized over to those of F-LUC-GFP, and set to 100% in Ctrl cells. Bars indicate the mean value, and error bars indicate the SD (n=3).

(E–J) Cells were transfected with *DBNDD2-HA* (E and G) or *LGALS3BP-HA* (F and H) (WT or $STOP_3$), treated with ActD, and harvested at the indicated time points. (E–H) Show representative northern blots. (I and J) mRNA levels were quantified, as described in Figure 2A. See also Figure S2.

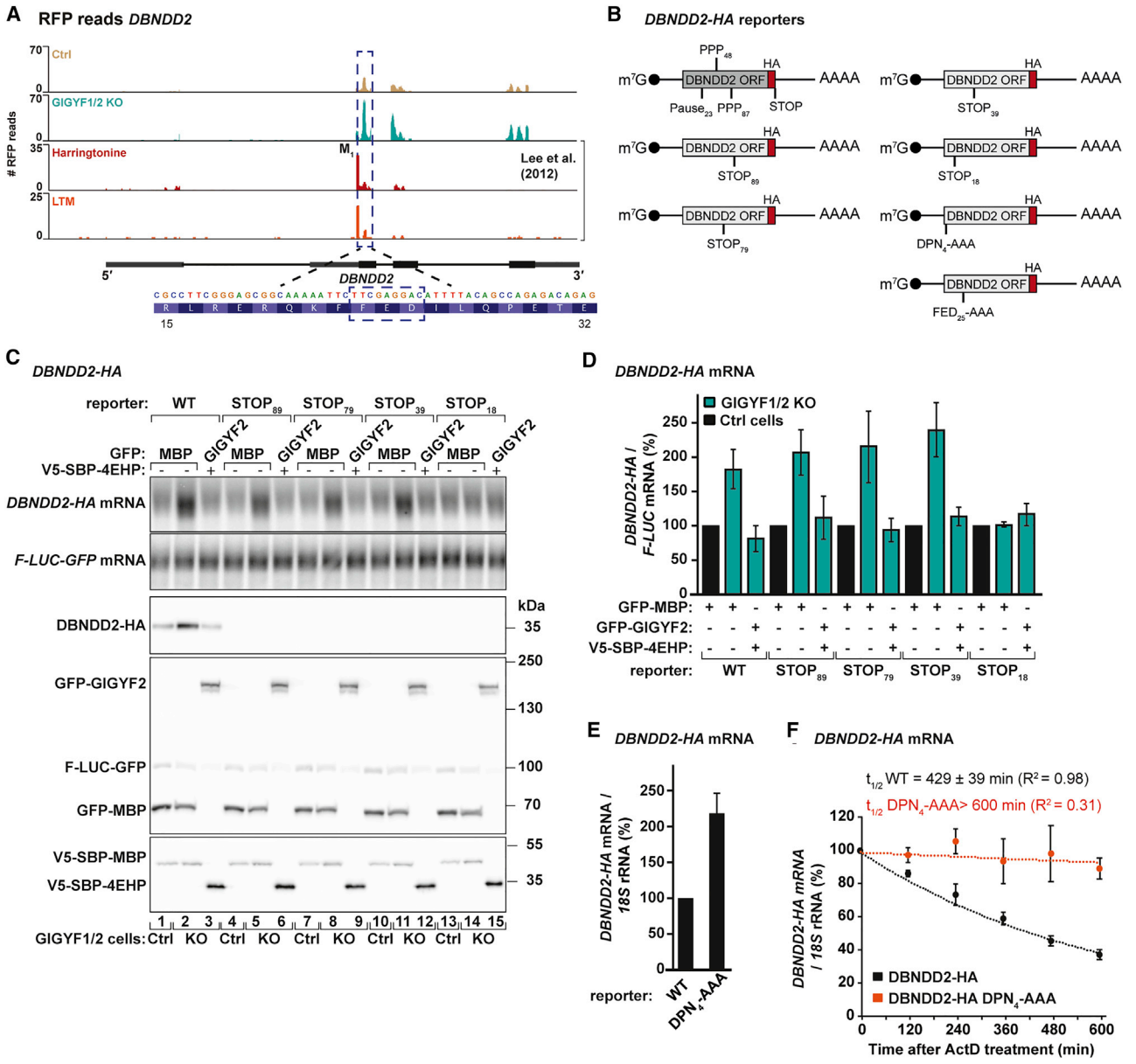

Figure 5. Ribosome Pausing Triggers GIGYF1/2-Dependent mRNA Decay

(A) RFP profiles of *DBNDD2* in Ctrl, GIGYF1/2 KO, and cells treated with harringtonine and lactimidomycin (LTM) (Lee et al., 2012). Dashed blue box highlights ribosome pausing. Gene annotation, protein sequence, and residue numbering are depicted below the profiles. M_1, Met_1.

(B) Schematic representation of the *DBNDD2-HA* reporters. $Pause_{23}$, position of the stall peptide (FED_{25}); PPP_{48} and PPP_{87}, poly-Pro motifs. STOPs were introduced 18, 39, 79, and 89 codons after the AUG. Alanine substitutions were inserted at the stall site and at the N terminus of the protein (DPN_4).

(C and D) Ctrl and GIGYF1/2 KO cells were transfected with *DBNDD2-HA* (WT or STOPs) and *F-LUC-GFP*. Cells were also co-transfected with GFP-MBP or GFP-GIGYF2 and V5-SBP-4EHP. mRNA levels were determined by northern blotting (C), normalized to *F-LUC-GFP*, and set to 100% in Ctrl cells (D). Bars indicate the mean value and error bars the SD (n = 3). The immunoblot with the expression of the GFP-, HA-, and V5-tagged proteins is also shown.

(E) Cells were transfected with *DBNDD2-HA* (WT or DPN_4-AAA). Reporter mRNA levels were quantified by qRT-PCR, normalized over to those of 18S rRNA, and set to 100% for *DBNDD2-HA* WT. Bars indicate the mean value and error bars the SD (n = 3).

(F) Cells transfected with *DBNDD2-HA* (WT or DPN_4-AAA) were treated with ActD and harvested at the indicated time points. mRNA levels were quantified by qRT-PCR as described in Figure 2A. See also Figures S4 and S6.

synthesis of the SP and co-translational ER targeting of LGALS3BP-HA.

GIGYF2 also efficiently associated with the *LGALS3BP-HA* mRNA (Figures 6E and 6F). Binding to the mRNA was greatly impaired if a STOP codon was present at the beginning of the CDS (*$STOP_3$*) to prevent the synthesis and exposure of the SP (Figures 4A and 6F). These results suggest that GIGYF2 interacts with translating *LGALS3BP* mRNA.

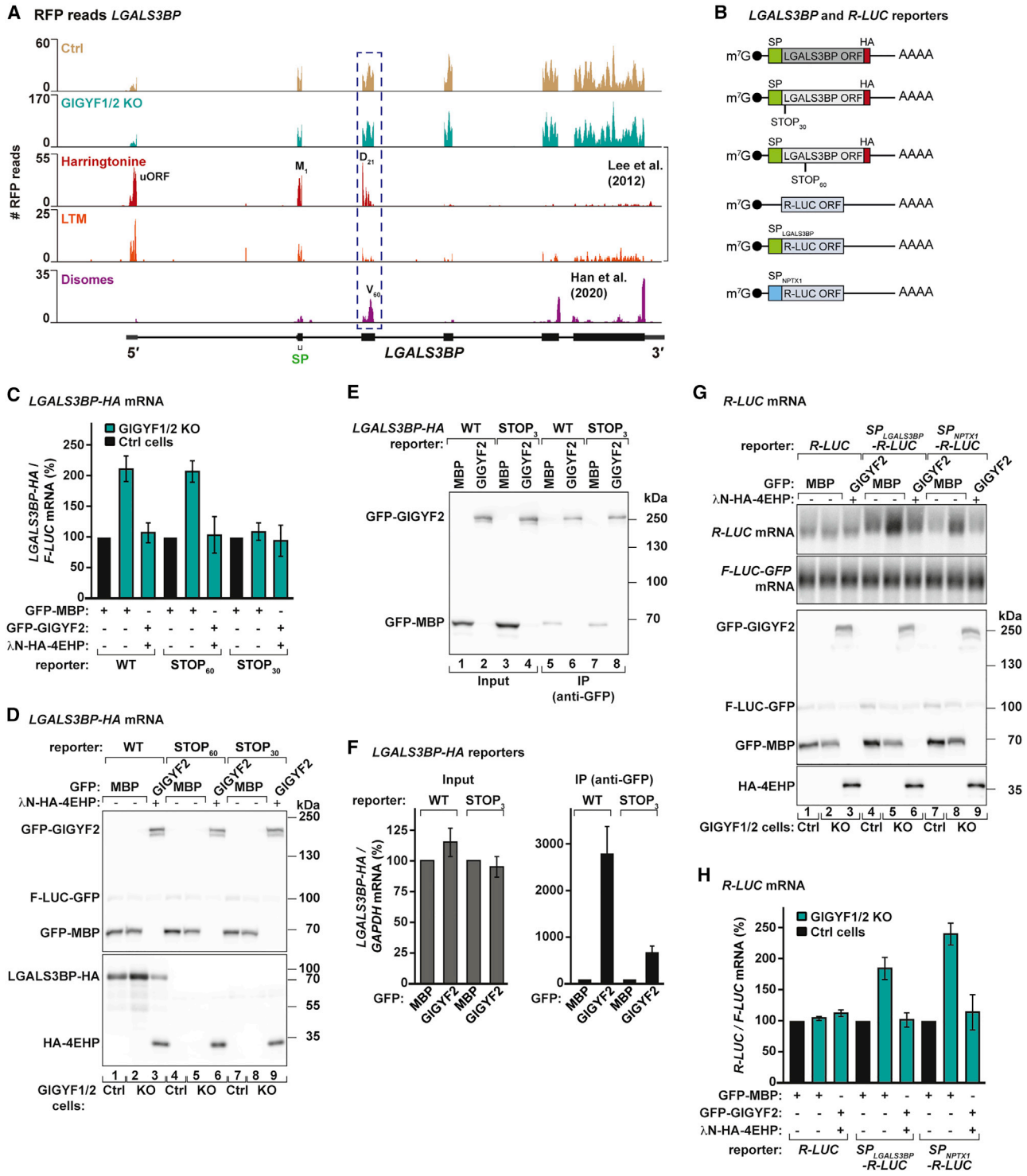

Figure 6. GIGYF1/2 Induce Co-translational Decay of Secretome mRNAs

(A) RFP profiles for *LGALS3BP* in Ctrl and GIGYF1/2 KO cells and in the presence of harringtonine or LTM (Lee et al., 2012). Disome occurrence along the CDS (Han et al., 2020) is also shown. Gene annotation is depicted below the profiles. M_1, Met_1; D_{21}, Asp_{21}; V_{60}, Val_{60}; uORF, upstream ORF.

(B) Schematic representation of the *LGALS3BP-HA* and *R-LUC* reporters. STOPs were introduced 30 and 60 codons after the AUG in *LGALS3BP-HA*. The signal sequences of the LGALS3BP and NPTX1 SPs were inserted upstream and in frame with the R-LUC CDS.

(C) *LGALS3BP-HA* (WT and STOPs) mRNA levels were measured by qRT-PCR in samples obtained from cells co-transfected with F-LUC-GFP, GFP-MBP, or GFP-GIGYF2, and λN-HA-4EHP. mRNA levels were set to 100% in Ctrl cells after normalization to *F-LUC-GFP*. Bars indicate the mean value; error bars represent SD (n = 3).

(legend continued on next page)

We then tested if the presence of the SP was sufficient to induce GIGYF1/2-dependent co-translational mRNA decay. We transfected cells with chimeric reporters in which R-LUC is in frame with the SP sequences of LGALS3BP or NPTX1 (Figure 6B). In comparison, the abundance of $SP_{LGALS3BP}$-*R-LUC* and SP_{NPTX1}-*R-LUC* mRNAs increased in GIGYF1/2 null cells (Figures 6G, lanes 5 and 8, and 6H). Re-expression of GIGYF2 and 4EHP was sufficient to decrease transcript levels in the null cells (Figures 6G, lanes 6 and 9, and 6H). In contrast, *R-LUC* abundance did not vary in the absence of GIGYF1/2 (Figures 6G, lanes 1–3, and 6H).

Collectively, these data support a model in which binding of GIGYF1/2 to a subset of secretome transcripts induces co-translational mRNA turnover. GIGYF1/2-mediated mRNA degradation is most likely favored by changes in elongation during synthesis of the SP.

Tubulin mRNAs Are Regulated by GIGYF1/2

Tubulin mRNAs are co-translationally degraded in cells with excess soluble subunits (Cleveland et al., 1981; Lin et al., 2020). *TUBA4A* and *TUBB4A* are 4EHP and GIGYF1/2 target mRNAs (Tables S2, S3, and S4). Using qRT-PCR, we confirmed that *TUBA4A* and *TUBB4A* abundance, but not *TUBB*, increased in GIGYF1/2 null cells (Figures 7A–7C). Consistent with a role of the complex in tubulin mRNA degradation, selective reduction of *TUBA4A* and *TUBB4A* levels was achieved in the null cells by re-expression of 4EHP and GIGYF2 (Figures 7A and 7B). Furthermore, *TUBA4A* was efficiently bound by GIGYF2 in a GYF-domain-dependent manner (Figure 7D).

Next, we examined if GIGYF1/2 regulate mRNA abundance in response to the level of free tubulin subunits. Pre-treatment of Ctrl cells with the microtubule destabilizing agent nocodazole elicited the decay of several tubulin mRNAs, as their levels dropped considerably (60%–75%) (Figures 7E–7I). In the absence of GIGYF1/2, nocodazole-induced decay only reduced mRNA levels by 35%–50% (Figures 7E–7I), suggesting that GIGYF1/2 may contribute to tubulin autoregulation. However, as 4EHP and GIGYF1/2 regulate mRNA turnover also in the absence of nocodazole (Figures 7A and 7B), further studies are required to address their effect in the control of tubulin levels in cells.

While tubulin autoregulation occurs co-translationally (Gay et al., 1989; Pachter et al., 1987), it remains unclear if the underlying mechanism is coupled with translational surveillance. Conventional ribosome profiling does not uncover ribosome pausing in tubulin mRNAs (Figures 7J and 7K). However, an analysis of ribosome footprints following run off assays (Lee et al., 2012) and disome profiling (Han et al., 2020; Tuck et al., 2020) shows that stalling and collision are frequent in *TUBA4A, TUBA1A*, and *TUBA1B* (Figures 7J, 7K, and S7A–S7D). Interestingly, the stalled and collided ribosomes are positioned 20 to 30 amino acids after the N-terminal motif of tubulins with a critical role in autoregulation (Figures 7J, 7K, and S7A–S7D; Pachter et al., 1987; Yen et al., 1988). Based on the ~35-residue length of the exit tunnel, the N-termini of tubulins would start to emerge from the ribosome. These observations suggest that 4EHP and GIGYF1/2 trigger the decay of tubulin mRNAs with perturbed translation elongation.

Collectively, our work shows that recognition of the nascent peptide by surveillance factors and detection of ribosome pausing and collisions during translation trigger GIGYF1/2-dependent mRNA decay (Figure S7E).

DISCUSSION

This study shows that 4EHP and GIGYF1/2 are selective regulators of mRNA turnover. Targeted transcripts frequently encode membrane-bound and secreted proteins, implicating 4EHP and GIGYF1/2 in the regulation of a subset of secretome mRNAs. Degradation is coupled with translation and is triggered by changes in ribosome activity during elongation. This function expands the role of the complex as a regulator of gene expression beyond the 3′ UTR-directed mechanisms operating during inflammation or miRNA-mediated gene silencing (Fu et al., 2016; Schopp et al., 2017; Tollenaere et al., 2019). Our findings have multiple implications for both translational control and mRNA decay and open future research directions.

Co-translational mRNA Decay by GIGYF1/2 Proteins

We find that co-translational mRNA degradation requires the coordinated action of several GIGYF1/2 co-factors. Binding and mRNA selection rely on GYF domain interacting proteins, such as ZNF598 that recruits 4EHP and GIGYF1/2 to destabilize transcripts marked by ribosome collisions. An alternate mode of selection relies on the recruitment of GIGYF1/2 by translation surveillance factors that recognize the nascent peptide as it emerges from the ribosome exit tunnel. Future studies will identify the surveillance factors synchronizing the recognition of the nascent chain with altered ribosome activity and the recruitment of the 4EHP-GIGYF1/2 complexes. The diversity of mechanisms for target recognition centralized on GIGYF1/2 proteins opens the possibility that mRNA decay is subject to regulation.

GIGYF1/2-directed recruitment of 4EHP to the cap not only reduces translation initiation but also facilitates the activity of the decay machinery. The reduced cap affinity of 4EHP compared with that of eIF4E (Chapat et al., 2017; Peter et al., 2017; Rom et al., 1998; Zuberek et al., 2007) exposes the mRNA to decapping (Ruscica et al., 2019). A scenario in which the recruitment of deadenylation and decapping factors by GIGYF1/2 occurs co-

(D) Analysis of GFP and HA protein expression by immunoblotting.
(E and F) The interaction of GFP-GIGYF2 with *LGALS3BP-HA* mRNA was analyzed in coIP assays by using anti-GFP antibodies. GFP-MBP served as a negative control. Input (0.2% for the GFP proteins and 0.7% for LGALS3BP-HA) and immunoprecipitated fractions (2.7% for the GFP proteins and 5% for LGALS3BP-HA) were analyzed by western blotting with anti-GFP antibodies. In (F), *LGALS3BP-HA* (WT or $STOP_3$) mRNA abundance in input (0.8%) and IP samples (12%) was quantified by qRT-PCR, normalized to *GAPDH*, and set to 100% in the presence of MBP. Bars represent the mean value and error bars the SD (n = 3).
(G and H) *R-LUC*, $SP_{LGALS3BP}$-*R-LUC*, or SP_{NPTX1}-*R-LUC* mRNAs were quantified by northern blotting in cells expressing F-LUC-GFP, GFP-MBP or GFP-GIGYF2, and λN-HA-4EHP. Normalized mRNA levels were set to 100% in Ctrl cells. Bars indicate the mean value and error bars the SD (n = 3). The expression of the GFP- and HA-tagged proteins was assessed by immunoblotting and is shown below the northern blot.

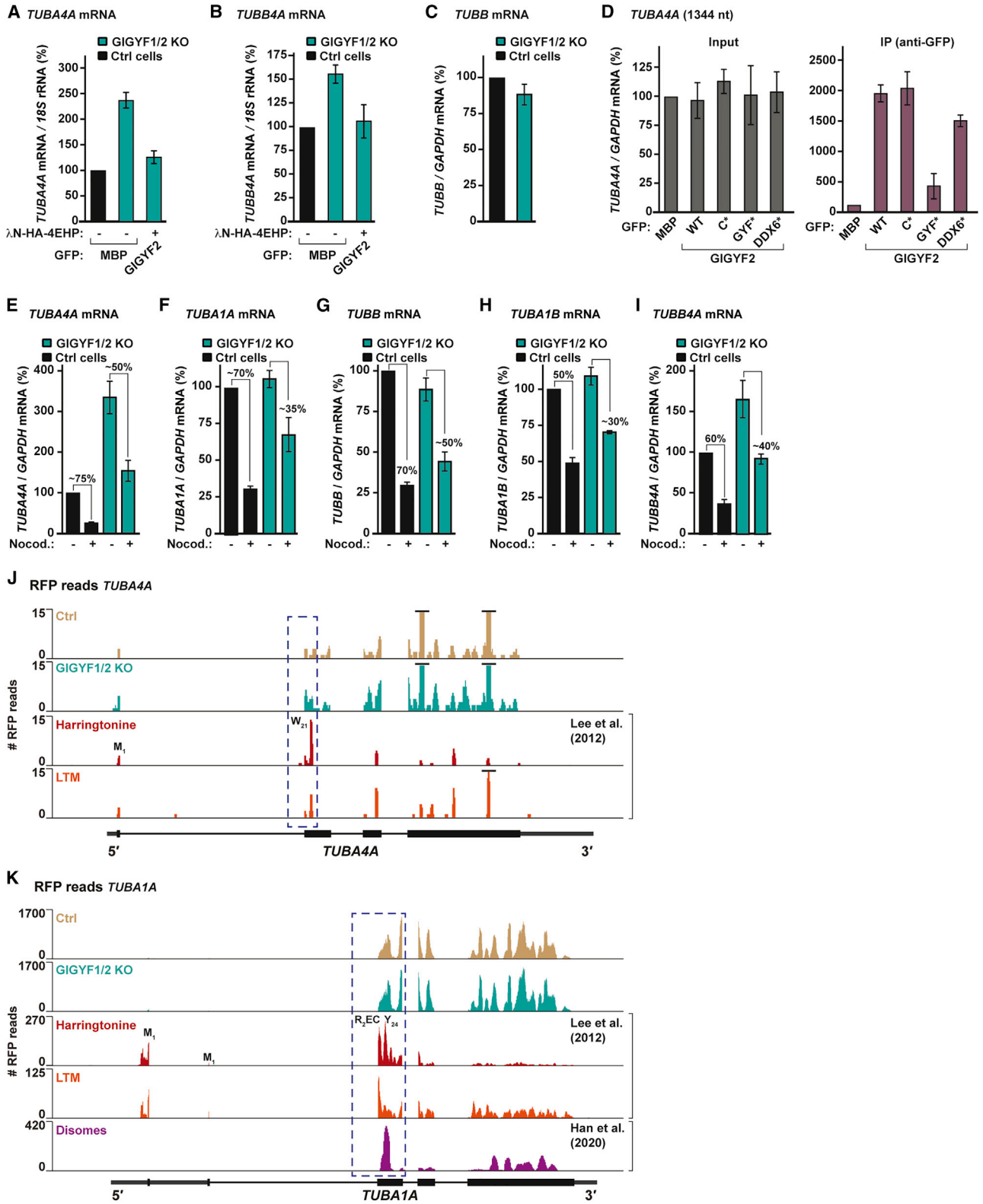

Figure 7. GIGYF1/2 Participate in Tubulin Co-translational mRNA Decay

(A–C) Cells were transfected with GFP-MBP or GFP-GIGYF2 and λN-HA-4EHP. Tubulin mRNA levels were quantified by qRT-PCR, normalized to those of *18S* rRNA (A and B) or *GAPDH* mRNA (C), and set to 100% in Ctrl cells. Plotted is the mean ± SD (n = 3).

(legend continued on next page)

translationally is in agreement with the ribosomal association and activity of decay factors, such as DDX6 (Sweet et al., 2012), the CCR4-NOT complex (Buschauer et al., 2020), and XRN1 (Pelechano et al., 2015; Tesina et al., 2019; Tuck et al., 2020), and would irreversibly prevent the translation of transcripts with impaired elongation.

Our data further support a role for DDX6 in GIGYF1/2-dependent mRNA decay and suggest that this RNA helicase might also monitor ribosome speed in the targeted transcripts, as demonstrated for mRNAs with poor codon optimality (Radhakrishnan et al., 2016).

GIGYF1/2 Mediate mRNA Decay in Response to Disturbed Elongation

Here, we present evidence that perturbed ribosome dynamics during elongation triggers canonical mRNA degradation by GIGYF1/2. Ribosome pausing and queuing prevailed in 4EHP and GIGYF1/2 target mRNAs. Pause sites included known stalling sequences and were associated with factors recognizing the nascent peptide. Co-translational target mRNA decay was in part mediated by ZNF598, a sensor of ribosome collisions, and in the absence of ribosome stalling, the abundance of target-based reporter transcripts was no longer regulated by GIGYF1/2. In addition, degradation of some of the GIGYF1/2 targets, such as tubulins and secretome mRNAs, is known to be dependent on translation and ribosome-associated factors (Cleveland et al., 1981; Karamyshev et al., 2014; Lakshminarayan et al., 2020; Lin et al., 2020).

Our findings suggest a model for which selective recruitment of 4EHP and GIGYF1/2 to mRNAs with altered elongation promotes translation repression and mRNA degradation. Target selection involves the recognition of stalled ribosomes by specialized co-factors and/or of the nascent peptide by surveillance proteins (Figure S7E). In line with the recruitment of 4EHP and GIGYF1/2 to mRNAs with failed translation events, while our work was under review, different studies revealed that ribosome collisions trigger the inhibition of translation initiation by 4EHP and GIGYF2 (Hickey et al., 2020; Juszkiewicz et al., 2020; Sinha et al., 2020). In this context, EDF1 (endothelial differentiation-related factor 1) facilitates the recruitment of 4EHP-GIGYF2 to the stalled ribosomes (Juszkiewicz et al., 2020; Sinha et al., 2020). Additional studies are warranted to understand the contribution of EDF1 to 4EHP- and GIGYF1/2-dependent co-translational mRNA decay.

GIGYF1/2 and Disease

Translation-dependent canonical mRNA degradation has been implicated in different cellular events. Autoregulation of tubulin mRNA abundance is crucial for proper cell division (Lin et al., 2020). Moreover, mutations in the autoregulatory domain of TUBB4A that abolish translation-coupled mRNA decay have been described in hereditary dystonia (Hersheson et al., 2013). As shown in this work, 4EHP and GIGYF1/2 participate in the turnover of different tubulin mRNAs. Additional studies are now required to identify the precise mechanism that links the recruitment of the 4EHP-GIGYF1/2 complex and the binding of TTC5 to the tubulin nascent peptide when cells activate autoregulation (Lin et al., 2020). Furthermore, our findings suggest that in the absence of GIGYF1/2, cells might be more prone to defects in division.

Co-translational mRNA decay likewise guarantees the quality of secretory and membrane proteins. To reduce the accumulation of misfolded and potentially toxic proteins, failure in protein targeting to the ER elicits degradation of the ribosome-bound message (Karamyshev et al., 2014; Lakshminarayan et al., 2020; Pinarbasi et al., 2018). Here, we identified the 4EHP-GIGYF1/2 complex as a member of the quality control system that regulates the turnover of a subset of secretome-associated mRNAs during co-translational assembly in the ER. We propose that 4EHP and GIGYF1/2 could likewise be important to trigger the degradation of specific mRNAs when the SP has reduced ability for ER targeting or folding. Given its ability to associate with polysomes and ribosomal proteins, one possibility is that like SRP (Voorhees and Hegde, 2015), GIGYF1/2 is co-translationally recruited at the initial stages of protein synthesis, scanning translating ribosomes as the SP elongates through the exit tunnel and interferes with the translation cycle. If ER targeting fails, GIGYF1/2 are then posed to elicit decay of the translating mRNA, avoiding the accumulation of misfolded proteins.

Although the causal mechanisms remain unknown, GIGYF1/2 loss and haploinsufficiency are associated with neurodegeneration and neurological disorders in animal models and affected humans (Giovannone et al., 2009; Iossifov et al., 2014; Krumm et al., 2015; Satterstrom et al., 2020; Schizophrenia Working Group of the Psychiatric Genomics Consortium, 2014; Thyme et al., 2019). Our work reports a previously unappreciated role of GIGYF1/2 in safeguarding the integrity of the proteome by signaling to conventional decay mRNAs with altered ribosome progression. This function of GIGYF1/2 proteins prevents the synthesis of unwanted or potentially cytotoxic proteins and, if compromised, may contribute to the development of neurological diseases.

Limitations

Our work highlights 4EHP and GIGYF1/2 as regulators of co-translational mRNA decay. To extend our observations to disease-related contexts, identification of the transcripts and ribosome-associated mechanisms regulated by 4EHP and

(D) GIGYF2 binding to *TUBA4A* mRNA was determined by RNA-IP, as described in Figure 3.

(E–I) Cells were treated with either DMSO (−) or nocodazole (+) for 3 h. Tubulin mRNA abundance was quantified by qRT-PCR, normalized to *GAPDH*, and set to 100% in the absence of nocodazole. Plotted is the mean ± SD (n = 3). Brackets indicate the approximate reduction in mRNA abundance following nocodazole treatment.

(J and K) RFP profiles of *TUBA4A* and *TUBA1A* in Ctrl, GIGYF1/2 KO, and cells treated with harringtonine or LTM (Lee et al., 2012). The *TUBA1A* profile also shows the distribution of disome footprints along the CDS (Han et al., 2020). Dashed squares identify paused ribosomes and disomes. In *TUBA4A* RFP, the black horizontal lines indicate footprint peaks that result from non-unique reads with nucleotide sequences common to multiple tubulin subunits. These footprints were not considered as ribosome pauses. M_1, Met_1; W_{21}, Trp_{21}; R_2, Arg_2; E, Glu; C, Cys; Y_{24}, Tyr_{24}. See also Figure S7.

GIGYF1/2 in models of human neurological pathologies and ER-related stress is still necessary. Such studies will greatly increase our knowledge on how translation-coupled mRNA decay tunes the cellular proteome.

STAR★METHODS

Detailed methods are provided in the online version of this paper and include the following:

- KEY RESOURCES TABLE
- RESOURCE AVAILABILITY
  - Lead Contact
  - Materials Availability
  - Data and Code Availability
- EXPERIMENTAL MODEL AND SUBJECT DETAILS
  - Cell lines
- METHOD DETAILS
  - DNA constructs
  - Generation of the 4EHP null and ZNF598 null cell lines
  - Ribosome profiling and RNA sequencing
  - Data analysis
  - Transfections, northern and western blotting
  - Reverse transcription (RT) and quantitative PCR (qPCR)
  - Half-life experiments
  - Polysome profiling
  - RNA immunoprecipitation/pulldown
  - Co-immunoprecipitation (Co-IP) assays
  - UPF1 Knockdown
- QUANTIFICATION AND STATISTICAL ANALYSES

SUPPLEMENTAL INFORMATION

Supplemental Information can be found online at https://doi.org/10.1016/j.celrep.2020.108262.

ACKNOWLEDGMENTS

We dedicate this work to the memory of Elisa Izaurralde. We gratefully acknowledge that the study was conceived and carried out in her laboratory. We are thankful to Nisar Malek and Przemyslaw Bozko for sharing nocodazole. We thank the Izaurralde lab members, Daniel Peter, and Dipankar Bandhari for helpful discussions on the manuscript. This work was supported by the Max Planck Society.

AUTHOR CONTRIBUTIONS

R.W. designed and conducted the experiments and was assisted by M.-Y.C. and C.K.; U.Z. and M.L. helped with Ribo-seq and RNA-seq experiments and contributed to data analysis; and E.V. contributed to data analysis. E.I. was the principle investigator. R.W. and C.I. conceived the project, interpreted the results, and wrote the manuscript. All authors, with exception of E.I., read and corrected the manuscript.

The authors declare no competing interests.

Received: February 18, 2020
Revised: August 26, 2020
Accepted: September 22, 2020
Published: October 13, 2020

REFERENCES

Amaya Ramirez, C.C., Hubbe, P., Mandel, N., and Béthune, J. (2018). 4EHP-independent repression of endogenous mRNAs by the RNA-binding protein GIGYF2. Nucleic Acids Res. *46*, 5792–5808.

Arpat, A.B., Liechti, A., De Matos, M., Dreos, R., Janich, P., and Gatfield, D. (2020). Transcriptome-wide sites of collided ribosomes reveal principles of translational pausing. Genome Res. *30*, 985–999.

Ash, M.R., Faelber, K., Kosslick, D., Albert, G.I., Roske, Y., Kofler, M., Schuemann, M., Krause, E., and Freund, C. (2010). Conserved beta-hairpin recognition by the GYF domains of Smy2 and GIGYF2 in mRNA surveillance and vesicular transport complexes. Structure *18*, 944–954.

Brandman, O., and Hegde, R.S. (2016). Ribosome-associated protein quality control. Nat. Struct. Mol. Biol. *23*, 7–15.

Buschauer, R., Matsuo, Y., Sugiyama, T., Chen, Y.H., Alhusaini, N., Sweet, T., Ikeuchi, K., Cheng, J., Matsuki, Y., Nobuta, R., et al. (2020). The Ccr4-Not complex monitors the translating ribosome for codon optimality. Science *368*, eaay6912.

Buskirk, A.R., and Green, R. (2017). Ribosome pausing, arrest and rescue in bacteria and eukaryotes. Philos. Trans. R. Soc. Lond. B Biol. Sci. *372*, 20160183.

Calviello, L., Mukherjee, N., Wyler, E., Zauber, H., Hirsekorn, A., Selbach, M., Landthaler, M., Obermayer, B., and Ohler, U. (2016). Detecting actively translated open reading frames in ribosome profiling data. Nat. Methods *13*, 165–170.

Chapat, C., Jafarnejad, S.M., Matta-Camacho, E., Hesketh, G.G., Gelbart, I.A., Attig, J., Gkogkas, C.G., Alain, T., Stern-Ginossar, N., Fabian, M.R., et al. (2017). Cap-binding protein 4EHP effects translation silencing by microRNAs. Proc. Natl. Acad. Sci. USA *114*, 5425–5430.

Cleveland, D.W., Lopata, M.A., Sherline, P., and Kirschner, M.W. (1981). Unpolymerized tubulin modulates the level of tubulin mRNAs. Cell *25*, 537–546.

D'Orazio, K.N., Wu, C.C., Sinha, N., Loll-Krippleber, R., Brown, G.W., and Green, R. (2019). The endonuclease Cue2 cleaves mRNAs at stalled ribosomes during No Go Decay. eLife *8*, e49117.

Doerfel, L.K., Wohlgemuth, I., Kothe, C., Peske, F., Urlaub, H., and Rodnina, M.V. (2013). EF-P is essential for rapid synthesis of proteins containing consecutive proline residues. Science *339*, 85–88.

Fu, R., Olsen, M.T., Webb, K., Bennett, E.J., and Lykke-Andersen, J. (2016). Recruitment of the 4EHP-GYF2 cap-binding complex to tetraproline motifs of tristetraprolin promotes repression and degradation of mRNAs with AU-rich elements. RNA *22*, 373–382.

Gaidatzis, D., Lerch, A., Hahne, F., and Stadler, M.B. (2015). QuasR: quantification and annotation of short reads in R. Bioinformatics *31*, 1130–1132.

Gardin, J., Yeasmin, R., Yurovsky, A., Cai, Y., Skiena, S., and Futcher, B. (2014). Measurement of average decoding rates of the 61 sense codons in vivo. eLife *3*, e03735.

Garreau de Loubresse, N., Prokhorova, I., Holtkamp, W., Rodnina, M.V., Yusupova, G., and Yusupov, M. (2014). Structural basis for the inhibition of the eukaryotic ribosome. Nature *513*, 517–522.

Garzia, A., Jafarnejad, S.M., Meyer, C., Chapat, C., Gogakos, T., Morozov, P., Amiri, M., Shapiro, M., Molina, H., Tuschl, T., and Sonenberg, N. (2017). The E3 ubiquitin ligase and RNA-binding protein ZNF598 orchestrates ribosome quality control of premature polyadenylated mRNAs. Nat. Commun. *8*, 16056.

Gasic, I., Boswell, S.A., and Mitchison, T.J. (2019). Tubulin mRNA stability is sensitive to change in microtubule dynamics caused by multiple physiological and toxic cues. PLoS Biol. *17*, e3000225.

Gay, D.A., Sisodia, S.S., and Cleveland, D.W. (1989). Autoregulatory control of beta-tubulin mRNA stability is linked to translation elongation. Proc. Natl. Acad. Sci. USA *86*, 5763–5767.

Gerbracht, J.V., Boehm, V., and Gehring, N.H. (2017). Plasmid transfection influences the readout of nonsense-mediated mRNA decay reporter assays in human cells. Sci. Rep. *7*, 10616.

Giovannone, B., Tsiaras, W.G., de la Monte, S., Klysik, J., Lautier, C., Karashchuk, G., Goldwurm, S., and Smith, R.J. (2009). GIGYF2 gene disruption in mice results in neurodegeneration and altered insulin-like growth factor signaling. Hum. Mol. Genet. *18*, 4629–4639.

Gutierrez, E., Shin, B.S., Woolstenhulme, C.J., Kim, J.R., Saini, P., Buskirk, A.R., and Dever, T.E. (2013). eIF5A promotes translation of polyproline motifs. Mol. Cell *51*, 35–45.

Han, P., Shichino, Y., Schneider-Poetsch, T., Mito, M., Hashimoto, S., Udagawa, T., Kohno, K., Yoshida, M., Mishima, Y., Inada, T., and Iwasaki, S. (2020). Genome-wide Survey of Ribosome Collision. Cell Rep. *31*, 107610.

Hanson, G., and Coller, J. (2018). Codon optimality, bias and usage in translation and mRNA decay. Nat. Rev. Mol. Cell Biol. *19*, 20–30.

Hermesh, O., and Jansen, R.P. (2013). Take the (RN)A-train: localization of mRNA to the endoplasmic reticulum. Biochim. Biophys. Acta *1833*, 2519–2525.

Hersheson, J., Mencacci, N.E., Davis, M., MacDonald, N., Trabzuni, D., Ryten, M., Pittman, A., Paudel, R., Kara, E., Fawcett, K., et al. (2013). Mutations in the autoregulatory domain of β-tubulin 4a cause hereditary dystonia. Ann. Neurol. *73*, 546–553.

Hickey, K.L., Dickson, K., Cogan, J.Z., Replogle, J.M., Schoof, M., D'Orazio, K.N., Sinha, N.K., Hussmann, J.A., Jost, M., Frost, A., et al. (2020). GIGYF2 and 4EHP Inhibit Translation Initiation of Defective Messenger RNAs to Assist Ribosome-Associated Quality Control. Mol. Cell *79*, 950–962.e6.

Hu, W., Sweet, T.J., Chamnongpol, S., Baker, K.E., and Coller, J. (2009). Co-translational mRNA decay in Saccharomyces cerevisiae. Nature *461*, 225–229.

Ikeuchi, K., Tesina, P., Matsuo, Y., Sugiyama, T., Cheng, J., Saeki, Y., Tanaka, K., Becker, T., Beckmann, R., and Inada, T. (2019). Collided ribosomes form a unique structural interface to induce Hel2-driven quality control pathways. EMBO J. *38*, e100276.

Ingolia, N.T., Ghaemmaghami, S., Newman, J.R., and Weissman, J.S. (2009). Genome-wide analysis in vivo of translation with nucleotide resolution using ribosome profiling. Science *324*, 218–223.

Ingolia, N.T., Lareau, L.F., and Weissman, J.S. (2011). Ribosome profiling of mouse embryonic stem cells reveals the complexity and dynamics of mammalian proteomes. Cell *147*, 789–802.

Ingolia, N.T., Brar, G.A., Rouskin, S., McGeachy, A.M., and Weissman, J.S. (2012). The ribosome profiling strategy for monitoring translation in vivo by deep sequencing of ribosome-protected mRNA fragments. Nat. Protoc. *7*, 1534–1550.

Iossifov, I., O'Roak, B.J., Sanders, S.J., Ronemus, M., Krumm, N., Levy, D., Stessman, H.A., Witherspoon, K.T., Vives, L., Patterson, K.E., et al. (2014). The contribution of de novo coding mutations to autism spectrum disorder. Nature *515*, 216–221.

Jan, C.H., Williams, C.C., and Weissman, J.S. (2014). Principles of ER cotranslational translocation revealed by proximity-specific ribosome profiling. Science *346*, 1257521.

Joazeiro, C.A.P. (2017). Ribosomal Stalling During Translation: Providing Substrates for Ribosome-Associated Protein Quality Control. Annu. Rev. Cell Dev. Biol. *33*, 343–368.

Joazeiro, C.A.P. (2019). Mechanisms and functions of ribosome-associated protein quality control. Nat. Rev. Mol. Cell Biol. *20*, 368–383.

Jonas, S., Weichenrieder, O., and Izaurralde, E. (2013). An unusual arrangement of two 14-3-3-like domains in the SMG5-SMG7 heterodimer is required for efficient nonsense-mediated mRNA decay. Genes Dev. *27*, 211–225.

Juszkiewicz, S., and Hegde, R.S. (2017). Initiation of Quality Control during Poly(A) Translation Requires Site-Specific Ribosome Ubiquitination. Mol. Cell *65*, 743–750.e744.

Juszkiewicz, S., Chandrasekaran, V., Lin, Z., Kraatz, S., Ramakrishnan, V., and Hegde, R.S. (2018). ZNF598 Is a Quality Control Sensor of Collided Ribosomes. Mol. Cell *72*, 469–481.e467.

Juszkiewicz, S., Slodkowicz, G., Lin, Z., Freire-Pritchett, P., Peak-Chew, S.Y., and Hegde, R.S. (2020). Ribosome collisions trigger cis-acting feedback inhibition of translation initiation. eLife *9*, e60038.

Karamyshev, A.L., Patrick, A.E., Karamysheva, Z.N., Griesemer, D.S., Hudson, H., Tjon-Kon-Sang, S., Nilsson, I., Otto, H., Liu, Q., Rospert, S., et al. (2014). Inefficient SRP interaction with a nascent chain triggers a mRNA quality control pathway. Cell *156*, 146–157.

Kim, D., Pertea, G., Trapnell, C., Pimentel, H., Kelley, R., and Salzberg, S.L. (2013). TopHat2: accurate alignment of transcriptomes in the presence of insertions, deletions and gene fusions. Genome Biol. *14*, R36.

Kowarik, M., Küng, S., Martoglio, B., and Helenius, A. (2002). Protein folding during cotranslational translocation in the endoplasmic reticulum. Mol. Cell *10*, 769–778.

Krumm, N., Turner, T.N., Baker, C., Vives, L., Mohajeri, K., Witherspoon, K., Raja, A., Coe, B.P., Stessman, H.A., He, Z.X., et al. (2015). Excess of rare, inherited truncating mutations in autism. Nat. Genet. *47*, 582–588.

Kryszke, M.H., Adjeriou, B., Liang, F., Chen, H., and Dautry, F. (2016). Post-transcriptional gene silencing activity of human GIGYF2. Biochem. Biophys. Res. Commun. *475*, 289–294.

Kuzuoğlu-Öztürk, D., Bhandari, D., Huntzinger, E., Fauser, M., Helms, S., and Izaurralde, E. (2016). miRISC and the CCR4-NOT complex silence mRNA targets independently of 43S ribosomal scanning. EMBO J. *35*, 1186–1203.

Labun, K., Montague, T.G., Gagnon, J.A., Thyme, S.B., and Valen, E. (2016). CHOPCHOP v2: a web tool for the next generation of CRISPR genome engineering. Nucleic Acids Res. *44*, W272–W276.

Labun, K., Montague, T.G., Krause, M., Torres Cleuren, Y.N., Tjeldnes, H., and Valen, E. (2019). CHOPCHOP v3: expanding the CRISPR web toolbox beyond genome editing. Nucleic Acids Res. *47*, W171–W174.

Lakshminarayan, R., Phillips, B.P., Binnian, I.L., Gomez-Navarro, N., Escudero-Urquijo, N., Warren, A.J., and Miller, E.A. (2020). Pre-emptive Quality Control of a Misfolded Membrane Protein by Ribosome-Driven Effects. Curr. Biol. *30*, 854–864.e5.

Langmead, B., and Salzberg, S.L. (2012). Fast gapped-read alignment with Bowtie 2. Nat. Methods *9*, 357–359.

Lazzaretti, D., Tournier, I., and Izaurralde, E. (2009). The C-terminal domains of human TNRC6A, TNRC6B, and TNRC6C silence bound transcripts independently of Argonaute proteins. RNA *15*, 1059–1066.

Lee, S., Liu, B., Lee, S., Huang, S.X., Shen, B., and Qian, S.B. (2012). Global mapping of translation initiation sites in mammalian cells at single-nucleotide resolution. Proc. Natl. Acad. Sci. USA *109*, E2424–E2432.

Lin, Z., Gasic, I., Chandrasekaran, V., Peters, N., Shao, S., Mitchison, T.J., and Hegde, R.S. (2020). TTC5 mediates autoregulation of tubulin via mRNA degradation. Science *367*, 100–104.

Livak, K.J., and Schmittgen, T.D. (2001). Analysis of relative gene expression data using real-time quantitative PCR and the 2(-Delta Delta C(T)) Method. Methods *25*, 402–408.

Manjunath, H., Zhang, H., Rehfeld, F., Han, J., Chang, T.C., and Mendell, J.T. (2019). Suppression of Ribosomal Pausing by eIF5A Is Necessary to Maintain the Fidelity of Start Codon Selection. Cell Rep. *29*, 3134–3146.e3136.

McCarthy, D.J., Chen, Y., and Smyth, G.K. (2012). Differential expression analysis of multifactor RNA-Seq experiments with respect to biological variation. Nucleic Acids Res. *40*, 4288–4297.

Montague, T.G., Cruz, J.M., Gagnon, J.A., Church, G.M., and Valen, E. (2014). CHOPCHOP: a CRISPR/Cas9 and TALEN web tool for genome editing. Nucleic Acids Res. *42*, 401–407.

Morita, M., Ler, L.W., Fabian, M.R., Siddiqui, N., Mullin, M., Henderson, V.C., Alain, T., Fonseca, B.D., Karashchuk, G., Bennett, C.F., et al. (2012). A novel 4EHP-GIGYF2 translational repressor complex is essential for mammalian development. Mol. Cell. Biol. *32*, 3585–3593.

Pachter, J.S., Yen, T.J., and Cleveland, D.W. (1987). Autoregulation of tubulin expression is achieved through specific degradation of polysomal tubulin mRNAs. Cell *51*, 283–292.

Paillusson, A., Hirschi, N., Vallan, C., Azzalin, C.M., and Mühlemann, O. (2005). A GFP-based reporter system to monitor nonsense-mediated mRNA decay. Nucleic Acids Res. *33*, e54.

Pavlov, M.Y., Watts, R.E., Tan, Z., Cornish, V.W., Ehrenberg, M., and Forster, A.C. (2009). Slow peptide bond formation by proline and other N-alkylamino acids in translation. Proc. Natl. Acad. Sci. USA *106*, 50–54.

Pelechano, V., and Alepuz, P. (2017). eIF5A facilitates translation termination globally and promotes the elongation of many non polyproline-specific tripeptide sequences. Nucleic Acids Res. *45*, 7326–7338.

Pelechano, V., Wei, W., and Steinmetz, L.M. (2015). Widespread Co-translational RNA Decay Reveals Ribosome Dynamics. Cell *161*, 1400–1412.

Peter, D., Igreja, C., Weber, R., Wohlbold, L., Weiler, C., Ebertsch, L., Weichenrieder, O., and Izaurralde, E. (2015). Molecular architecture of 4E-BP translational inhibitors bound to eIF4E. Mol. Cell *57*, 1074–1087.

Peter, D., Weber, R., Sandmeir, F., Wohlbold, L., Helms, S., Bawankar, P., Valkov, E., Igreja, C., and Izaurralde, E. (2017). GIGYF1/2 proteins use auxiliary sequences to selectively bind to 4EHP and repress target mRNA expression. Genes Dev. *31*, 1147–1161.

Peter, D., Ruscica, V., Bawankar, P., Weber, R., Helms, S., Valkov, E., Igreja, C., and Izaurralde, E. (2019). Molecular basis for GIGYF-Me31B complex assembly in 4EHP-mediated translational repression. Genes Dev. *33*, 1355–1360.

Pillai, R.S., Artus, C.G., and Filipowicz, W. (2004). Tethering of human Ago proteins to mRNA mimics the miRNA-mediated repression of protein synthesis. RNA *10*, 1518–1525.

Pinarbasi, E.S., Karamyshev, A.L., Tikhonova, E.B., Wu, I.H., Hudson, H., and Thomas, P.J. (2018). Pathogenic Signal Sequence Mutations in Progranulin Disrupt SRP Interactions Required for mRNA Stability. Cell Rep. *23*, 2844–2851.

Presnyak, V., Alhusaini, N., Chen, Y.H., Martin, S., Morris, N., Kline, N., Olson, S., Weinberg, D., Baker, K.E., Graveley, B.R., and Coller, J. (2015). Codon optimality is a major determinant of mRNA stability. Cell *160*, 1111–1124.

Radhakrishnan, A., and Green, R. (2016). Connections Underlying Translation and mRNA Stability. J. Mol. Biol. *428*, 3558–3564.

Radhakrishnan, A., Chen, Y.H., Martin, S., Alhusaini, N., Green, R., and Coller, J. (2016). The DEAD-Box Protein Dhh1p Couples mRNA Decay and Translation by Monitoring Codon Optimality. Cell *167*, 122–132.e129.

Ran, F.A., Hsu, P.D., Wright, J., Agarwala, V., Scott, D.A., and Zhang, F. (2013). Genome engineering using the CRISPR-Cas9 system. Nat. Protoc. *8*, 2281–2308.

Räsch, F., Weber, R., Izaurralde, E., and Igreja, C. (2020). 4E-T-bound mRNAs are stored in a silenced and deadenylated form. Genes Dev. *34*, 847–860.

Robinson, M.D., McCarthy, D.J., and Smyth, G.K. (2010). edgeR: a Bioconductor package for differential expression analysis of digital gene expression data. Bioinformatics *26*, 139–140.

Robinson, J.T., Thorvaldsdóttir, H., Winckler, W., Guttman, M., Lander, E.S., Getz, G., and Mesirov, J.P. (2011). Integrative genomics viewer. Nat. Biotechnol. *29*, 24–26.

Rom, E., Kim, H.C., Gingras, A.C., Marcotrigiano, J., Favre, D., Olsen, H., Burley, S.K., and Sonenberg, N. (1998). Cloning and characterization of 4EHP, a novel mammalian eIF4E-related cap-binding protein. J. Biol. Chem. *273*, 13104–13109.

Ruscica, V., Bawankar, P., Peter, D., Helms, S., Igreja, C., and Izaurralde, E. (2019). Direct role for the Drosophila GIGYF protein in 4EHP-mediated mRNA repression. Nucleic Acids Res. *47*, 7035–7048.

Satterstrom, F.K., Kosmicki, J.A., Wang, J., Breen, M.S., De Rubeis, S., An, J.Y., Peng, M., Collins, R., Grove, J., Klei, L., et al. (2020). Large-Scale Exome Sequencing Study Implicates Both Developmental and Functional Changes in the Neurobiology of Autism. Cell *180*, 568–584.e23.

Schizophrenia Working Group of the Psychiatric Genomics Consortium. (2014). Biological insights from 108 schizophrenia-associated genetic loci. Nature *511*, 421–427.

Schmidt, C., Becker, T., Heuer, A., Braunger, K., Shanmuganathan, V., Pech, M., Berninghausen, O., Wilson, D.N., and Beckmann, R. (2016). Structure of the hypusinylated eukaryotic translation factor eIF-5A bound to the ribosome. Nucleic Acids Res. *44*, 1944–1951.

Schneider, C.A., Rasband, W.S., and Eliceiri, K.W. (2012). NIH Image to ImageJ: 25 years of image analysis. Nat. Methods *9*, 671–675.

Schopp, I.M., Amaya Ramirez, C.C., Debeljak, J., Kreibich, E., Skribbe, M., Wild, K., and Béthune, J. (2017). Split-BioID a conditional proteomics approach to monitor the composition of spatiotemporally defined protein complexes. Nat. Commun. *8*, 15690.

Schuller, A.P., Wu, C.C., Dever, T.E., Buskirk, A.R., and Green, R. (2017). eIF5A Functions Globally in Translation Elongation and Termination. Mol. Cell *66*, 194–205.e195.

Simms, C.L., Thomas, E.N., and Zaher, H.S. (2017a). Ribosome-based quality control of mRNA and nascent peptides. Wiley Interdiscip. Rev. RNA *8*. https://doi.org/10.1002/wrna.1366.

Simms, C.L., Yan, L.L., and Zaher, H.S. (2017b). Ribosome Collision Is Critical for Quality Control during No-Go Decay. Mol. Cell *68*, 361–373.e365.

Sinha, N.K., Ordureau, A., Best, K., Saba, J.A., Zinshteyn, B., Sundaramoorthy, E., Fulzele, A., Garshott, D.M., Denk, T., Thoms, M., et al. (2020). EDF1 coordinates cellular responses to ribosome collisions. eLife *9*, e58828.

Sundaramoorthy, E., Leonard, M., Mak, R., Liao, J., Fulzele, A., and Bennett, E.J. (2017). ZNF598 and RACK1 Regulate Mammalian Ribosome-Associated Quality Control Function by Mediating Regulatory 40S Ribosomal Ubiquitylation. Mol. Cell *65*, 751–760.e754.

Sweet, T., Kovalak, C., and Coller, J. (2012). The DEAD-box protein Dhh1 promotes decapping by slowing ribosome movement. PLoS Biol. *10*, e1001342.

Tesina, P., Heckel, E., Cheng, J., Fromont-Racine, M., Buschauer, R., Kater, L., Beatrix, B., Berninghausen, O., Jacquier, A., Becker, T., and Beckmann, R. (2019). Structure of the 80S ribosome-Xrn1 nuclease complex. Nat. Struct. Mol. Biol. *26*, 275–280.

Thorvaldsdóttir, H., Robinson, J.T., and Mesirov, J.P. (2013). Integrative Genomics Viewer (IGV): high-performance genomics data visualization and exploration. Brief. Bioinform. *14*, 178–192.

Thyme, S.B., Pieper, L.M., Li, E.H., Pandey, S., Wang, Y., Morris, N.S., Sha, C., Choi, J.W., Herrera, K.J., Soucy, E.R., et al. (2019). Phenotypic Landscape of Schizophrenia-Associated Genes Defines Candidates and Their Shared Functions. Cell *177*, 478–491.e420.

Tollenaere, M.A.X., Tiedje, C., Rasmussen, S., Nielsen, J.C., Vind, A.C., Blasius, M., Batth, T.S., Mailand, N., Olsen, J.V., Gaestel, M., et al. (2019). GIGYF1/2-Driven Cooperation between ZNF598 and TTP in Posttranscriptional Regulation of Inflammatory Signaling. Cell Rep. *26*, 3511–3521.e3514.

Tuck, A.C., Rankova, A., Arpat, A.B., Liechti, L.A., Hess, D., Iesmantavicius, V., Castelo-Szekely, V., Gatfield, D., and Bühler, M. (2020). Mammalian RNA Decay Pathways Are Highly Specialized and Widely Linked to Translation. Mol. Cell *77*, 1222–1236.e13.

Voorhees, R.M., and Hegde, R.S. (2015). Structures of the scanning and engaged states of the mammalian SRP-ribosome complex. eLife *4*, e07975.

Walter, P., and Blobel, G. (1981). Translocation of proteins across the endoplasmic reticulum III. Signal recognition protein (SRP) causes signal sequence-dependent and site-specific arrest of chain elongation that is released by microsomal membranes. J. Cell Biol. *91*, 557–561.

Wohlgemuth, I., Brenner, S., Beringer, M., and Rodnina, M.V. (2008). Modulation of the rate of peptidyl transfer on the ribosome by the nature of substrates. J. Biol. Chem. *283*, 32229–32235.

Wolin, S.L., and Walter, P. (1988). Ribosome pausing and stacking during translation of a eukaryotic mRNA. EMBO J. *7*, 3559–3569.

Wolin, S.L., and Walter, P. (1989). Signal recognition particle mediates a transient elongation arrest of preprolactin in reticulocyte lysate. J. Cell Biol. *109*, 2617–2622.

Yen, T.J., Gay, D.A., Pachter, J.S., and Cleveland, D.W. (1988). Autoregulated changes in stability of polyribosome-bound beta-tubulin mRNAs are specified by the first 13 translated nucleotides. Mol. Cell. Biol. *8*, 1224–1235.

Young, M.D., Wakefield, M.J., Smyth, G.K., and Oshlack, A. (2010). Gene ontology analysis for RNA-seq: accounting for selection bias. Genome Biol. *11*, R14.

Zhong, Y., Karaletsos, T., Drewe, P., Sreedharan, V.T., Kuo, D., Singh, K., Wendel, H.G., and Rätsch, G. (2017). RiboDiff: detecting changes of mRNA translation efficiency from ribosome footprints. Bioinformatics *33*, 139–141.

Zuberek, J., Kubacka, D., Jablonowska, A., Jemielity, J., Stepinski, J., Sonenberg, N., and Darzynkiewicz, E. (2007). Weak binding affinity of human 4EHP for mRNA cap analogs. RNA *13*, 691–697.

STAR★METHODS

KEY RESOURCES TABLE

REAGENT or RESOURCE	SOURCE	IDENTIFIER
Antibodies		
Mouse monoclonal anti-GFP	Roche	Cat. #11814460001: RRID: AB_390913
Rabbit polyclonal anti-GFP	In house	N/A
Rabbit polyclonal anti-*Hs*GIGYF1	Bethyl laboratories	Cat. #A304-132A-M
Rabbit polyclonal anti-*Hs*GIGYF2	Bethyl laboratories	Cat. #A303-731A
Rabbit polyclonal anti-*Hs*ZNF598	Bethyl laboratories	Cat. #A305-108A
Rabbit polyclonal anti-*Hs*4EHP	In house	N/A
Mouse monoclonal anti-HA (HRP)	Roche	Cat. #12013819001: RRID: AB_390917
Mouse monoclonal anti-Tubulin	Sigma Aldrich	Cat. #T6199: RRID: AB_477583
Mouse monoclonal anti-V5	LSBio LifeSpan BioSciences, Inc.	Cat. #LS-C57305: RRID: AB_1512087
Anti-RENT1 (UPF1)	Bethyl laboratories	Cat. #A301-902A: RRID: AB_1524122
Anti-R-LUC	Abcam	Cat. #ab185925
Donkey polyclonal anti-rabbit IgG (HRP)	GE Healthcare	Cat. #NA934V
Sheep polyclonal anti-mouse IgG (HRP)	GE Healthcare	Cat. #RPN4201
Chemicals, Peptides, and Recombinant Proteins		
Lipofectamine 2000	Thermo Scientific	Cat. #11668-019
DMEM	In house	N/A
FBS	Thermo Scientific	Cat. #10270-106
Penicillin-Streptomycin	Thermo Scientific	Cat. #15140-122
L-Glutamine	Thermo Scientific	Cat. #25030-024
Agarose	Thermo Scientific	Cat. #16500-500
Low melting Agarose	Serva Electrophoresis	Cat. #11384
Phusion DNA polymerase	Thermo Scientific	Cat. #F-530XL
IgG beads	GE Healthcare	Cat. #17-0885-04
Streptavidin beads	GE Healthcare	Cat. #17-5113-01
TRIzol	Thermo Scientific	Cat. #15596018
TriFast FL	Peqlab Biotechnologies	Cat. #30-2120
P:C:I, stabilized	PanReac AppliChem	Cat. #A0889,0100
RiboLock	Thermo Scientific	Cat. #EO0381
dNTPs	Thermo Scientific	Cat. #R0141, #R0171, #R0161, #R0152
RevertAid H Minus reverse transcriptase	Thermo Scientific	Cat. #EP0451
Actinomycin D	Sigma Aldrich	Cat. #A9415
Puromycin	Serva Electrophoresis	Cat. #33835
Harringtonine	Sigma Aldrich	Cat. #SML1091
Protease Inhibitor (cOmplete, EDTA-free)	Roche	Cat. #05056489001
Yeast RNA	Roche	Cat. #10109223001
Nitrocellulose Transfer Membrane	Santa Cruz Biotechnology	Cat. #sc-3724
Luminol	Roth	Cat. #4203.1
P-Coumaric acid	Sigma Aldrich	Cat. #C9008
GeneScreen Plus nylon Membrane	Perkin Elmer	Cat. #NEF1018001PK
Cycloheximide	Serva Electrophoresis	Cat. #10700
Nocodazole	Sigma Aldrich	Cat #M1404
TurboDNase	Thermo Scientific	Cat. #AM2238
RNA Clean & Concentrator Kit	Zymo Research	Cat. #R1015

(*Continued on next page*)

Continued

REAGENT or RESOURCE	SOURCE	IDENTIFIER
Zymoclean Gel DNA Recovery Kit	Zymo Research	Cat. #D4007
MicroSpin S-400 HR Columns	GE Healthcare	Cat. #27514001
RNaseI	Thermo Scientific	Cat. #AM2294
SUPERase Inhibitor	Thermo Scientific	Cat. #AM2694
Ribo-Zero Gold rRNA Removal Kit	Illumina	discontinued
SYBR Gold	Thermo Scientific	Cat. #S11494
SuperScript II reverse transcriptase	Thermo Scientific	Cat. #18064014
SuperScript III reverse transcriptase	Thermo Scientific	Cat. #18080044
T4 Polynucleotide kinase	NEB	Cat. #M0201S
GlycoBlue	Thermo Scientific	Cat. #AM9515
T4 RNA Ligase 2, truncated K227Q	NEB	Cat. #M0351S
5′ DNA Adenylation Kit	NEB	Cat. #E2610S
T4 RNA Ligase 1	NEB	Cat. #M0204S
Critical Commercial Assays		
RNeasy Mini Kit	QIAGEN	Cat. #74104
Dual-luciferase reporter assay	Promega	Cat. #E1960
iTaq Sybr Green Supermix	Biorad	Cat. #170-8885
Wizard SV Genomic DNA Purification System	Promega	Cat. #A2360
TruSeq RNA sample Prep Kit	Illumina	Cat. #RS-122-2002
Deposited Data		
Raw and analyzed RNA-Seq and Ribo-Seq data – WT, 4EHP-null and GIGYF1/2-null HEK293T cells	This study	GEO: GSE144841
Raw and analyzed RNA-Seq and Ribo-Seq data – WT and ZNF598-null HEK293T cells	This study	GSE149279
Harringtonine and LTM treated HEK293 cells	Lee et al., 2012	SRA: SRA056377
Monosome and disome profiling of HEK293 cells	Han et al., 2020	GEO: GSE145723
Monosome and disome profiling in mESCs	Tuck et al., 2020	GEO: GSE134020
Source imaging data	This study – Mendeley data	https://doi.org/10.17632/dk55r385cj.1
Experimental Models: Cell Lines		
HEK293T	DSMZ	ACC 635
GIGYF1/2 KO	Peter et al., 2017	N/A
4EHP KO	Räsch et al., 2020	N/A
ZNF598 KO	This study	N/A
Oligonucleotides		
Oligonucleotides, see Table S7	This study	N/A
Recombinant DNA		
pλN-HA-C1-*Hs*eIF4E2 (4EHP)	Peter et al., 2017	Uniprot: O60573-1
pλN-HA-C1-*Hs*eIF4E2 W124A (cap*)	Peter et al., 2017	N/A
pλN-HA-C1-*Hs*eIF4E2 R103L, E149L (S*)	Peter et al., 2017	N/A
pT7-V5-SBP-C1-*Hs*eIF4E2 (4EHP)	Peter et al., 2017	N/A
pT7-V5-SBP- C1-*Hs*eIF4E2 W124A (cap*)	Peter et al., 2017	N/A
pT7-V5-SBP- C1-*Hs*eIF4E2 R103L, E149L (S*)	Peter et al., 2017	N/A
pT7-EGFP-C1-*Hs*GIGYF1	Peter et al., 2017	Uniprot: O60573-1

(*Continued on next page*)

Continued

REAGENT or RESOURCE	SOURCE	IDENTIFIER
pT7-EGFP-C1-*Hs*GIGYF1 Y39A Y41A M46A L47A (C*)	Peter et al., 2017	N/A
pT7-EGFP-C1-*Hs*GIGYF1 Y479A F490A W498A F504A (GYF*)	Peter et al., 2017	N/A
pT7-EGFP-C1-*Hs*GIGYF1 W294A, F306A, F312A (DDX6*)	Peter et al., 2019	N/A
pT7-EGFP-C1-*Hs*GIGYF2	Peter et al., 2017	Uniprot: Q6Y7W6-1
pT7-EGFP-C1-*Hs*GIGYF2 Y41A Y43A M48A L49A (C*)	Peter et al., 2017	N/A
pT7-EGFP-C1-*Hs*GIGYF2 Y538A, F549A, W557A, F563A (GYF*)	Peter et al., 2017	N/A
pT7-EGFP-C1-*Hs*GIGYF2 W288A, F300A, F306A (DDX6*)	Peter et al., 2019	N/A
pT7-EGFP-C1-*Hs*GIGYF2 C-term (719-1299)	This study	N/A
pEGFP-N3-F-Luc-EGFP	Lazzaretti et al., 2009	N/A
pCIneo-*Hs*DBNDD2-HA	This study	Uniprot: Q9BQY9-2
pCIneo-*Hs*DBNDD2-STOP$_3$-HA	This study	N/A
pCIneo-*Hs*DBNDD2-STOP$_{18}$-HA	This study	N/A
pCIneo-*Hs*DBNDD2-STOP$_{39}$-HA	This study	N/A
pCIneo-*Hs*DBNDD2-STOP$_{79}$-HA	This study	N/A
pCIneo-*Hs*DBNDD2-STOP$_{89}$-HA	This study	N/A
pCIneo-*Hs*DBNDD2-FED$_{25}$-AAA-HA	This study	N/A
pCIneo-*Hs*DBNDD2-DPN$_4$-AAA-HA	This study	N/A
pCIneo-R-Luc-*Hs*DBNDD2 3′ UTR	This study	N/A
pCIneo-*Hs*LGALS3BP-HA	This study	Uniprot: Q08380-1
pCIneo-*Hs*LGALS3BP-STOP$_3$-HA	This study	N/A
pCIneo-*Hs*LGALS3BP-STOP$_{30}$-HA	This study	N/A
pCIneo-*Hs*LGALS3BP-STOP$_{60}$-HA	This study	N/A
pCIneo-R-LUC-*Hs*LGALS3BP 3′ UTR	This study	N/A
pCIneo-*Hs* SP$_{LGALS3BP}$-R-LUC	This study	N/A
pCIneo-*Hs* SP$_{NPTX1}$-R-LUC	This study	N/A
pCIneo-R-LUC	Pillai et al., 2004	N/A
pSpCas9(BB)-2A-Puro (PX459)	Ran et al., 2013	Addgene 48139
pSUPERpuro-BglII-scrambled	Jonas et al., 2013	N/A
pSUPERpuro-BglII-HsUPF1-t2	Paillusson et al., 2005	N/A
pSUPERpuro-BglII-HsUPF1-t4	Paillusson et al., 2005	N/A
Software and Algorithms		
Adobe Illustrator	Adobe	https://www.adobe.com/uk/creativecloud.html
Integrative Genomics Viewer	Robinson et al., 2011; Thorvaldsdóttir et al., 2013	https://software.broadinstitute.org/software/igv/
ImageJ	Schneider et al., 2012	https://imagej.nih.gov/ij/
Bowtie 2	Langmead and Salzberg, 2012	http://bowtie-bio.sourceforge.net/bowtie2/index.shtml
TopHat 2	Kim et al., 2013	https://ccb.jhu.edu/software/tophat/index.shtml
RiboTaper	Calviello et al., 2016	https://ohlerlab.mdc-berlin.de/software/RiboTaper_126/

(*Continued on next page*)

Continued

REAGENT or RESOURCE	SOURCE	IDENTIFIER
QuasR	Gaidatzis et al., 2015	https://bioconductor.org/packages/release/bioc/html/QuasR.html
edgeR	McCarthy et al., 2012; Robinson et al., 2010	https://bioconductor.org/packages/release/bioc/html/edgeR.html
RiboDiff	Zhong et al., 2017	https://github.com/ratschlab/RiboDiff
goseq	Young et al., 2010	https://bioconductor.org/packages/release/bioc/html/goseq.html
CHOPCHOP	Labun et al., 2016, 2019; Montague et al., 2014	http://chopchop.cbu.uib.no

RESOURCE AVAILABILITY

Lead Contact

Further information and requests for resources and reagents should be directed to and will be fulfilled by the Lead Contact, Catia Igreja (catia.igreja@tuebingen.mpg.de).

Materials Availability

All unique/stable reagents generated in this study are available from the Lead Contact with a completed Materials Transfer Agreement.

Data and Code Availability

The accession numbers for the RNA-seq and Ribo-seq data in WT, 4EHP-null, GIGYF1/2-null and ZNF598-null HEK293T cells reported in this paper are Gene Expression Omnibus (GEO): GSE144841 and GSE149279). Original data have been deposited to Mendeley Data: https://doi.org/10.17632/dk55r385cj.1.

EXPERIMENTAL MODEL AND SUBJECT DETAILS

Cell lines

All cell lines were cultured at 37°C and 5% CO_2 in Dulbecco's Modified Eagle's Medium (DMEM) supplemented with 10% fetal bovine serum, 2 mM Glutamine, 1x Penicillin and 1x Streptomycin.

METHOD DETAILS

DNA constructs

DNA constructs used in this study are listed in the Key Resources Table. All plasmids used in the assays depicted in Figures 3 and S2, the *Renilla* luciferase (R-LUC) and the firefly luciferase (F-LUC)-EGFP reporters were described previously (Lazzaretti et al., 2009; Peter et al., 2017; Pillai et al., 2004). The UPF1 shRNA plasmids were a kind gift from Oliver Mühlemann (Paillusson et al., 2005). To generate the CDS reporters, the sequences of *DBNDD2* or the *LGALS3BP* ORFs were cloned into the NheI-XbaI restriction sites of the pCIneo vector. The C-terminal HA-tag was inserted by site-directed mutagenesis. The *DBNDD2-STOP-HA* reporters with UAA stop codons at various positions (3, 18, 39, 79 and 89 codons downstream of the AUG start site) and the *LGALS3BP-STOP-HA* reporters with UAA stop codons at various positions (3, 30 and 60 codons downstream of the AUG start site) were generated by mutagenesis. To obtain the 3′ UTR reporters, the sequences of *DBNDD2* or the *LGALS3BP* 3′ UTRs were cloned into the XhoI-NotI and XbaI-NotI restriction sites of the pCIneo-R-LUC vector, respectively. The eL22L1 (1-122) was cloned into the NheI-XbaI restriction sites of the pCIneo vector; the N-terminal V5-SBP sequence was inserted by mutagenesis. To generate the SP-R-LUC vectors the sequences corresponding to the signal peptides (as annotated by Uniprot) of LGALS3BP (1-18: MTPPRLFWVWLLVAGTQG) and NPTX1 (1-22: MPAGRAARTCALLALCLLGAGA) were cloned upstream of R-LUC ORF in the pCIneo-R-LUC vector by mutagenesis. All the mutants used in this study were generated by site-directed mutagenesis using the QuickChange Site-Directed Mutagenesis kit (Stratagene). All the constructs were confirmed by sequencing.

Generation of the 4EHP null and ZNF598 null cell lines

sgRNAs targeting 4EHP and ZNF598 were designed using the CHOPCHOP (http://chopchop.cbu.uib.no) online tool (Labun et al., 2016, 2019; Montague et al., 2014) and cloned into the pSpCas9(BB)-2A-Puro (PX459) vector [a gift from F. Zhang, Addgene plasmid 48139; (Ran et al., 2013)]. Clonal cell lines were obtained and confirmed for gene editing as described previously (Peter et al., 2017).

Briefly, HEK293T cells were transfected with the sgRNA-Cas9 vectors. Two days post transfection, cells were treated with puromycin (3 μg/ml; Serva Electrophoresis) to select for edited cells. Serial dilutions in 96-well plates were used to obtain single cell clones. Genomic DNA was isolated from single clones using the Wizard SV Genomic DNA Purification System (Promega). The 4EHP locus was PCR amplified and Sanger sequencing of the targeted genomic regions confirmed two frameshift mutations in exon 4 (an 11 nucleotide and a 37 nucleotide deletions) targeted by sg4EHP-a. For sg4EHP-b we did not observe gene editing; the amplified sequence around the target site in exon 2 is wild-type. The ZNF598 locus was targeted by sgZNF598-a (exon 3) and sgZNF598-b (exon 4). RNA sequencing shows that in ZNF598 KO cells genome editing resulted in the expression of a ZNF598 transcript that lacks exons 1-4 and retains intron 4 at the 5′ end. This transcript has reduced translation efficiency and is subject to degradation. The lack of 4EHP and ZNF598 expression was confirmed by western blotting (Figures S1A and S5A). See Table S7 for sgRNA sequences.

Ribosome profiling and RNA sequencing

HEK293T (DSMZ, ACC 635) wild-type, GIGYF1/2 null (Peter et al., 2017), 4EHP null (Räsch et al., 2020) and ZNF598 null cells were plated on 10 cm dishes 24 hours before harvesting, as previously described (Calviello et al., 2016). Cells were lysed with lysis buffer (20 mM Tris-HCl pH = 7.4, 150 mM NaCl, 5 mM $MgCl_2$, 1 mM DTT, 1% Triton X-100, 0.5% NP40) containing cyclohexamide (100 μg/ml). Lysates were then used for total RNA extraction and ribosome profiling (1/4 of the lysate for each). Total RNA was extracted using the RNeasy Mini Kit (50) (QIAGEN) after pre-treating the lysate with 10 U TurboDNase (Thermo Scientific). cDNA libraries were prepared using the TruSeq RNA Sample Prep Kit (Illumina), according to the manufacturers' instructions.

Ribosome profiling was performed according to the original protocol (Ingolia et al., 2012) with the modifications described in Calviello et al. (2016). Cell lysates were treated with 300 U RNase 1 (Thermo Scientific). Reactions were stopped after 45 min incubation at room temperature by adding 80 U SUPERase Inhibitor (Thermo Scientific). The RNase 1-treated samples were applied to MicroSpin S-400 HR columns (GE Healthcare) to remove free nucleotides and recover the ribosome-protected RNA. RNA extraction was then performed with TriFast FL (Peqlab Biotechnologies) and the RNA Clean & Concentrator Kit (Zymo Research). rRNA was depleted using the Ribo-Zero Gold rRNA Depletion Kit (Illumina, discontinued). Ribosome footprints were excised and extracted from a 17% TBE-Urea gel using 30 and 27 nt RNA oligonucleotides as markers. Ribosome footprints were treated with T4 PNK (NEB) and purified using P:C:I (PanReac AppliChem). 3′ and 5′ adapters were ligated using T4 RNA ligase 2, truncated K227Q (NEB) and T4 RNA ligase 1 (NEB), respectively. Following adaptor ligation, the resulting ribosome footprints were excised and extracted from a 15% TBE-Urea gel. Adaptor-ligated ribosome footprints were reversed transcribed with SuperScript III (Thermo Scientific). cDNA was PCR amplified using Phusion DNA polymerase (Thermo Scientific). PCR amplicons were visualized on a 2.5% low melting agarose (Serva Electrophoresis), excised and purified using the Zymoclean Gel DNA Recovery Kit (Zymo Research). DNA and sample quality were assessed using the Bioanalyzer system (Agilent). The sequences of the oligonucleotides used in this protocol are listed in Table S7.

Two biological replicates were analyzed. The ribosome profiling and total RNA libraries were sequenced using the Hiseq 3000 sequencing system (Illumina). Ribosomal RNA reads were filtered using Bowtie 2 (Langmead and Salzberg, 2012). Remaining reads were mapped on the hg19 (UCSC) human genome with TopHat2 (Kim et al., 2013). For RNA sequencing, 17.0-21.5 million reads were mapped (> 87%). Ribosome profiling reads were analyzed for three-nucleotide periodicity using the RiboTaper program to identify actively translating ribosomes (Calviello et al., 2016). Reads corresponding to the lengths of 29 and 30 nucleotides were selected as they showed the most significant three nucleotide periodicity and were then used for subsequent mapping on the human genome with TopHat2. For ribosome profiling, 6.1-9.6 million reads (> 95%) of input reads were mapped. Read count analysis was performed with the R/Bioconductor package QuasR (Gaidatzis et al., 2015). Differential expression analysis and multidimensional scaling (MDS) analysis were conducted using edgeR (McCarthy et al., 2012; Robinson et al., 2010) for selected genes with a threshold of 'fragments per kilobase of transcript per million mapped reads' (FPKM) > 2. Translation efficiency (TE) was calculated with the RiboDiff program (Zhong et al., 2017).

Harringtonine and LTM datasets from human HEK293 cells were downloaded from the Sequence Read Archive database (accession: SRA056377). The mouse ESC disome and human HEK293 cells disome datasets were retrieved from the GEO database. The respective accession numbers are GSE134020 and GSE145723. Ribosomal RNA reads were filtered using Bowtie 2 (Langmead and Salzberg, 2012). The remaining reads were mapped on the hg19 (UCSC) human genome or the mm9 (UCSC) mouse genome with TopHat2 (Kim et al., 2013). No specific filters for read length were applied.

Data analysis

Upregulated and downregulated gene groups were defined as being significantly regulated (FDR < 0.005) with a $\log_2FC > 0$ and $\log_2FC < 0$, respectively. No cutoff on the $\log_2FC$ value was applied so that genes with little but significant changes could also be detected. GO analysis was performed with the R based package GOseq (Young et al., 2010). The % of genes within each category corresponds to the number of genes belonging to the category and upregulated in the null cells divided by the total number of upregulated genes in HEK293T cells.

UniProt information was retrieved to analyze the presence of a signal peptide or the cellular location of the proteins encoded by 4EHP and GIGYF1/2 target mRNAs. Ribosome footprint density plots for individual sequencing tracks were visualized using the Integrative Genomics Viewer (IGV) visualization tool (Robinson et al., 2011; Thorvaldsdóttir et al., 2013).

Ribosome pause scores were determined for each of the common and upregulated mRNAs in 4EHP- and GIGYF1/2 null cells. Maximum (pause site) and median RFP coverage in the CDS of each transcript was retrieved using UCSC annotation and

Ribo-Seq data in GIGYF1/2 null cells replicate number 1. The pause score refers to the reads at the pause position divided by median reads in the gene. The values are listed in Table S4.

Transfections, northern and western blotting

In the rescue assays described in Figures 3, 5, 6, 7, S2, and S3, 0.64 × 10^6 Ctrl cells or 0.7 × 10^6 null cells were transfected, after seeding in 6-well plates, using Lipofectamine 2000 (Invitrogen). The transfection mixtures contained different amounts of the plasmids expressing λN-HA- or V5-SBP-fusion proteins (**λN-HA/V5-SBP-MBP**: 0.25 μg; **4EHP**: 0.25 μg of WT and cap* mutant, or 0.35 μg of S* mutant) and the GFP-fusion proteins (**MBP**: 0.4 μg, **GIGYF1**: 0.5 μg of WT, C*, GYF* and DDX6* mutants; **GIGYF2**: 1.75 μg of WT, 1.1 μg of C* or 1.35 μg of GYF* and DDX6* mutants). In the experiments shown in Figures 4, 5, and 6, the transfection mixtures contained plasmids expressing DBNDD2-HA, DBNDD2-$STOP_x$-HA, DBNDD2-FDE_{25}-AAA-HA or DBNDD2-DPN_4-AAA-HA (0.2 μg), and LGALS3BP-HA, LGALS3BP-$STOP_x$-HA, R-LUC, $SP_{LGALS3BP}$-R-LUC or SP_{NPTX1}-R-LUC (0.5 μg). In the assay with the 3′ UTR reporters, the transfection mixtures contained 0.5 μg of R-LUC-DBNDD2-3′ UTR, R-LUC-LGALS3BP-3′ UTR or R-LUC, and 0.25 μg of F-LUC-GFP plasmid DNA.

Cells were harvested two days after transfection and firefly and *Renilla* luciferase activities were measured using the Dual-Luciferase reporter assay system (Promega). Total RNA was isolated using TriFast (Peqlab biotechnologies). For Northern blotting, total RNA was separated in 2% glyoxal agarose gels and blotted onto a positively charged nylon membrane (GeneScreen Plus, Perkin Elmer). [^{32}P]-labeled probes specific for each transcript were generated by linear PCR. Hybridizations were carried out in hybridization solution (0.5 M NaP pH = 7.0, 7% SDS, 1 mM EDTA pH = 8.0) at 65°C overnight. After extensive washes with washing solution (40 mM NaP pH = 7.0, 1% SDS, 1 mM EDTA pH = 8.0), the membranes were exposed and band intensities were quantified by PhosphoImager. For detection of *DBNDD2* and *LGALS3BP* cellular and reporter mRNAs, complementary and radioactively labeled probes were designed against the CDS of the transcripts. Since the reporter constructs only harbor the CDS but no 5′ and 3′ sequences, the endogenous mRNAs are expected to run slower on an agarose gel. We observed that the signal of the transfected reporters is considerably stronger and does not allow the simultaneous detection of cellular and reporter mRNAs.

To test for tubulin mRNA autoregulation, control and GIGYF1/2 null HEK293T cells were grown to 70 % confluency and treated with nocodazole (10 μM, Sigma Aldrich) or DMSO for 3 hours as described previously (Lin et al., 2020). RNA was extracted using TRIzol (Thermo Scientific), reverse-transcribed and analyzed by quantitative PCR (qPCR; 10% of each RNA sample) as described below.

Western blot was performed using standard methods. In brief, cells were washed with PBS and lysed with sample buffer (100 mM Tris-HCl pH = 6.8, 4% SDS, 20% glycerol, 0.2 M DTT) followed by boiling 5 minutes at 95°C and vortexing to shear genomic DNA. After SDS-PAGE, proteins were transferred onto a nitrocellulose membrane (Santa Cruz Biotechnology) by tank transfer. Primary antibodies were incubated overnight at 4°C, secondary antibodies for an hour at room temperature. All western blots were developed with freshly mixed 10A: 1B ECL solutions and 0.01% H_2O_2 [Solution A: 0.025 % Luminol (Roth) in 0.1 M Tris-HCl pH = 8.6; Solution B: 0.11% P-Coumaric acid (Sigma Aldrich) in DMSO]. Antibodies used in this study are listed in the Key Resources Table. DBNDD2-HA and LGALS3BP-HA band intensities were quantified using ImageJ (Schneider et al., 2012) and normalized to the band intensities of F-LUC-GFP protein in the same experiment.

Reverse transcription (RT) and quantitative PCR (qPCR)

1 μg of RNA was mixed with 0.66 μg random hexamer primers (N_6) and denatured at 72°C for 5 min. After addition of a reaction mixture containing a final concentration of 1x RT buffer, 20 U RiboLock RNase Inhibitor (Thermo Scientific) and 1 mM dNTPs, the RNA samples were incubated at 37°C for 5 min. Incubation with RevertAid H Minus Reverse Transcriptase (200 U, Thermo Scientific) was first performed for 10 min at 25°C, and then at 42°C for one hour. The RT reaction was stopped by incubating the samples for 10 min at 70°C. The qPCR was performed with 1x iTaq SYBR Green Supermix (Biorad), 0.4 μM of each primer and 1 μl of the cDNA sample. mRNA levels were determined by qPCR using sequence-specific primers for the indicated transcripts and normalized to *18S* rRNA or *GAPDH* mRNA abundance in the same sample. qPCR primers designed using Primer-BLAST (NCBI) are listed in Table S7. Normalized transcript expression ratios from three independent experiments were determined using the Livak method (Livak and Schmittgen, 2001).

Half-life experiments

To measure mRNA decay rates, cells were treated with Actinomycin D (10 μg/ml final concentration) two days post transfection or three days after seeding and collected at the indicated time points. mRNA levels determined by Northern blotting or qPCR were normalized to the levels of *TUBB* or *18S* rRNA, respectively. Steady state *TUBB* mRNA levels remain unchanged in the absence of GIGYF1/2 (Figure 7C). These values were set to 100 at time point zero. Data points from three independent experiments were plotted and the resulting fitting curves were determined using a one phase exponential decay equation. The R^2 values associated with the fitting of the exponential decay curves were between 0.29 and 0.99. The curves with low R^2 indicate that reduction of mRNA levels over time are not well represented by an exponential decay model whereas high R^2 values indicate that the quantity of mRNA decreases at a rate proportional to its current value. To determine the time required for the decaying quantity to fall to half of its initial value, or half-life, a decay curve was first determined for each replica. The three values were then averaged to have the final half-life value. The three values were also used to determine the error (standard deviation) associated with the measurements. The standard deviation in the half-live values therefore reflects how reproducible the three replicas were.

Polysome profiling

Polysome profiles were performed as described before (Kuzuoğlu-Öztürk et al., 2016). HEK293T cells were pretreated with cycloheximide (50 μg/ml) for 30 min. Lysates were prepared in lysis buffer (10 mM Tris-HCl pH = 7.4, 10 mM NaCl, 1.5 mM $MgCl_2$, 0.5% Triton X-100, 2 mM DTT, 50 μg/ml cycloheximide) and polysomes separated on a 10%–50% sucrose gradient in gradient buffer (10 mM Tris-HCl pH 7.4, 75 mM KCl, 1.5 mM $MgCl_2$). Polysome fractions were collected using the Teledyne Isco Density Gradient Fractionation System. Protein from sucrose fractions was isolated by methanol extraction. In detail, 4x volumes of MetOH were mixed with the sucrose fractions, then mixed with 1x volume of chloroform and then with 3x volumes of water. After centrifugation, the upper phase was removed leaving the lower and inter-phases which were precipitated using 3x volumes of MetOH. Samples were spun down and the dried pellet dissolved in 2x protein sample buffer. Fractions were analyzed by western blotting.

RNA immunoprecipitation/pulldown

To immunoprecipitate GIGYF2-bound mRNA, 3 × 10^6 HEK293T cells were transfected using Lipofectamine 2000 (Invitrogen) 24 hours after seeding in 10 cm plates. The transfection mixtures contained the plasmid expressing the GFP-fusion proteins (MBP: 2.5 μg, **GIGYF2**: 10 μg of WT, 6 μg of C*, 12 μg of GYF* and 10 μg DDX6* mutants). In Figure S3, the RNA-IP was performed in cells treated with 2 μg/ml harringtonine for 30 min or 200 μg/ml puromycin for 45 min. In Figure 6, GFP-tagged MBP or GIGYF2 were co-expressed with LGALS3BP-HA or LGALS3BP-$STOP_3$-HA (5 μg). To pulldown 4EHP-bound mRNA (Figure S2), cells were co-transfected with the plasmids encoding V5-SBP-fusion proteins (MBP: 1 μg, **4EHP**: 12 μg of WT together with MBP and GIGYF2 C*, or 0.5 μg together with GIGYF2 WT, GYF* and DDX6*) and GFP-fusion proteins (MBP: 1 μg, **GIGYF2**: 5 μg of WT and DDX6*, 4 μg of C* and 8 μg of GYF* mutants). Cells were harvested 48 hours post transfection, washed with ice cold PBS and lysed on ice for 15 minutes in 500 μL of NET buffer [50 mM Tris-HCl pH = 7.5, 150 mM NaCl, 0.1% Triton X-100, 1 mM EDTA pH = 8.0, 10 % glycerol, supplemented with 1x protease inhibitors (Roche)]. Cell debris was removed by centrifugation at 16,000 *g* at 4°C. Input samples (5% of the total) were collected for western blotting and qRT-PCR. To immunoprecipitate GFP-GIGYF2, the remaining lysate was then incubated with 3 μL of anti-GFP antibody (homemade) for an hour, followed by incubation (2 hours) with protein G Sepharose resin pre-treated with yeast RNA (250 μg of yeast RNA/100 μL of 50% slurry). For pulldown of SBP-V5-4EHP and associated RNA, cell lysates were immediately incubated with 50 μL of a 50% slurry of streptavidin beads pre-incubated with yeast RNA. Beads were washed 3 times with NET buffer and ressuspended in 1 mL of NET buffer without detergent. An aliquot (20% of the total) of the bead suspension, was mixed with SDS-PAGE sample buffer for western blotting after centrifugation to pellet the resin. The remaining beads were used for RNA isolation with TriFast (Peqlab Biotechnologies). cDNA of the input and precipitated fractions (20% each) was prepared and analyzed using qPCR (5% of the cDNA) as described above.

Co-immunoprecipitation (Co-IP) assays

Co-IP assays were performed in the presence of RNase A as described previously (Peter et al., 2015). HEK293T cells were grown in 10 cm dishes and transfected using Lipofectamine 2000 (Invitrogen) according to the manufacturer's recommendations. The transfection mixtures in Figures S1I and S1J contained 2.5 μg of GFP-MBP or GFP-GIGYF1 WT, 3 μg of GFP-GIGYF1 GYF*, 10 μg of GFP-GIGYF2 WT or 12 μg of GFP-GIGYF2 GYF*. In Figure S3B, GFP-MBP or GFP-GIGYF2 were co-expressed with V5-SBP-eL22L1 (5 μg). After transfection, cells were treated as described in the RNA-IP section, with the exception that the protein G Sepharose resin was not incubated with yeast RNA and the samples were only used for protein analysis.

UPF1 Knockdown

In the reporter assays described in Figures S6B, S6C, and S6F, 0.64 × 10^6 Ctrl cells were transfected with 2 μg pSUPER-puro scramble control or UPF1 shRNA, after seeding in 6-well plates, using Lipofectamine 2000 (Invitrogen). 24 hours after transfection cells were treated with 5 μM puromycin for 24 hours. Selected cells were re-seeded and re-transfected with the transfection mixtures described above (Transfections, northern and western blotting section).

QUANTIFICATION AND STATISTICAL ANALYSES

Figures 1A, 1B, S5B, and S5C. Upregulated and downregulated genes were identified using log_2Fold Change (FC) between null and control cells > 0 or < 0, respectively, and False Discovery Rates (FDR) < 0.005.

Figures 1C, S1G, and S5F. The hypergeometric test (phyper) in R was applied to estimate the likelihood of list overlap.

Figures 1D and 1E. The quantitative value represented in the graphs corresponds to -log_{10}(q-value) determined by the GOseq analysis tool (Young et al., 2010).

Figures 2, 4, 5, and S5. Dots represent mean value; error bars represent the standard deviation from three independent experiments. The mRNA decay curves were fitted to an exponential decay with a single component. R^2 values are indicated for each curve.

Figures 3, 4, 5, 6, 7, S2, S3, S4, and S6. The quantitative value that is graphed represents the mean mRNA or protein level values; error bars represent standard deviations from three independent experiments. In the qRT-PCR experiments, normalized transcript expression ratios from three independent experiments were determined using the Livak method (Livak and Schmittgen, 2001).

Cell Reports, Volume *33*

Supplemental Information

4EHP and GIGYF1/2 Mediate Translation-Coupled Messenger RNA Decay

Ramona Weber, Min-Yi Chung, Csilla Keskeny, Ulrike Zinnall, Markus Landthaler, Eugene Valkov, Elisa Izaurralde, and Cátia Igreja

Weber *et al.* Figure S1

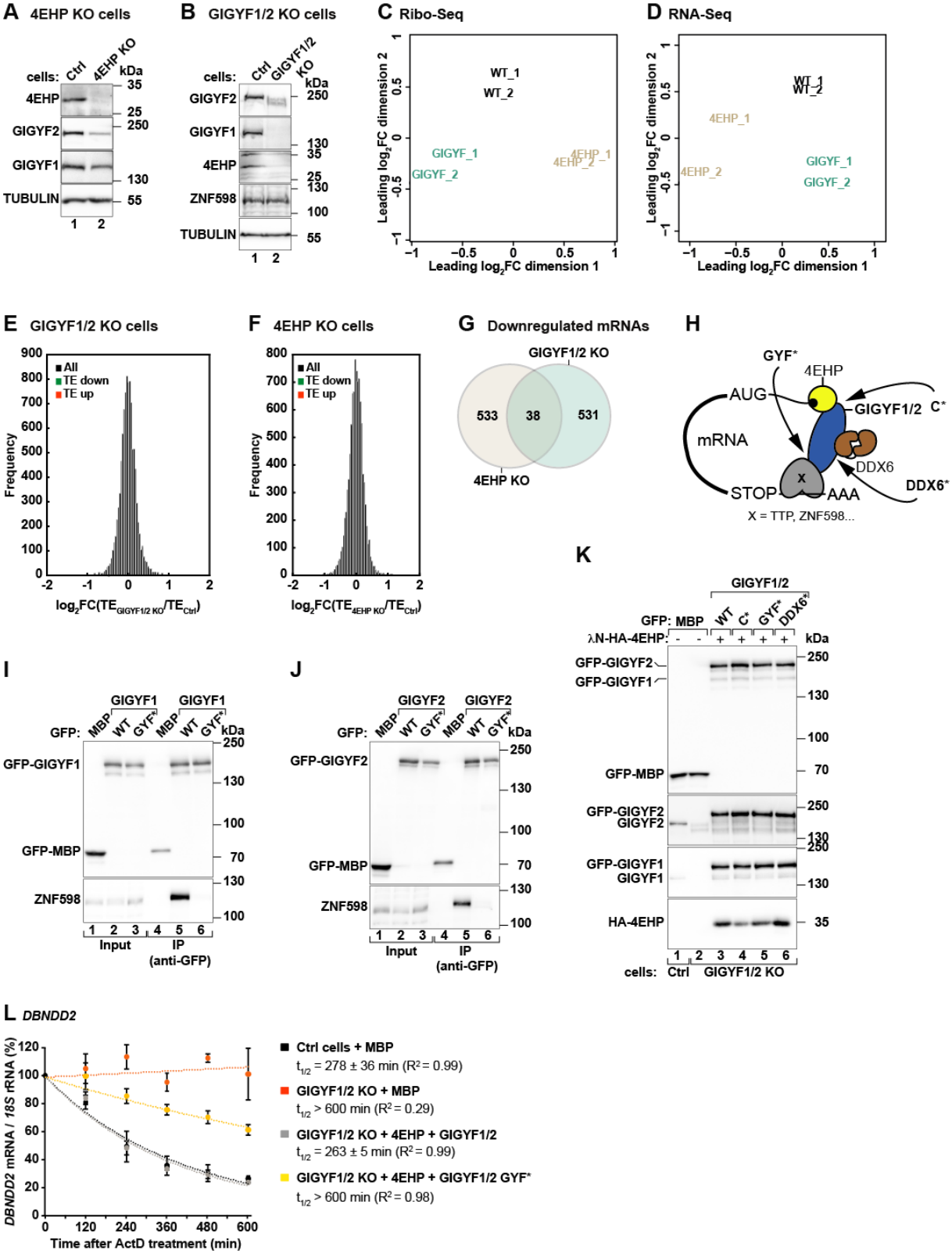

Figure S1, related to Figures 1 and 3. Characterization of 4EHP-null (KO) and GIGYF1/2-null cells

(A, B) Western blots demonstrating loss of endogenous 4EHP in 4EHP KO cells (A) and endogenous GIGYF1 and GIGYF2 in GIGYF1/2 KO cells (B). GIGYF1 and GIGYF2 expression is reduced in 4EHP KO cells and

4EHP is weakly expressed in GIGYF1/2 KO cells. TUBULIN served as loading control. Note that the TUBULIN antibody recognizes an epitope common among the α-tubulin subunits of which TUBA4A and TUBA1A are genes with increased mRNA abundance in 4EHP-null cells.

(C, D) Multidimensional scaling (MDS) analysis for the Ribo-Seq replicate libraries (C) and the RNA-Seq replicate libraries (D) from HEK293T WT, GIGYF1/2-null and 4EHP-null cells.

(E, F) Histograms of the number of transcripts (frequency) relative to the $\log_2$FC of translational efficiency (TE) in GIGYF1/2 null (E) and 4EHP null cells (F). Significantly upregulated (FDR<0.005 and $\log_2$FC>0) transcripts are depicted in orange, significantly downregulated (FDR<0.005 and $\log_2$FC<0) transcripts are shown in green. There were only few genes with changes in TE (Table S1).

(G) Venn diagram of the genes with decreased mRNA abundance (downregulated genes) in GIGYF1/2 null and 4EHP null cells identifies a non-significant overlap of 38 transcripts.

(H) Schematic representation of the effector complex involved in GIGYF1/2-mediated mRNA decay. GIGYF1/2 canonical (C*) mutant is unable to interact with 4EHP; GIGYF1/2 DDX6* protein does not associate with the RNA helicase DDX6; the GIGYF1/2 GYF* mutant cannot interact with PPGΦ-rich proteins. TTP: tristetraprolin; X: RNA-binding protein.

(I, J) The interaction of GIGYF1 (I) and GIGYF2 (J) WT or GYF domain mutant (GYF*) with ZNF598 was analyzed in co-immunoprecipitation assays using anti-GFP antibodies. GFP-MBP served as a negative control. The input (0.8% for the GFP proteins and 0.3% for ZNF598) and immunoprecipitated fractions (12% for the GFP proteins and 24% for ZNF598) were analyzed by western blotting with anti-GFP and anti-ZNF598 antibodies.

(K) Immunoblot showing the expression of the proteins used in the experiment depicted in Figures 3A, B. Blots were probed with antibodies recognizing GFP, GIGYF1, GIGYF2 or HA. Inputs and immunoprecipitates were 2% and 2.7%, respectively.

(L) Ctrl and GIGYF1/2 KO cells were transfected with plasmids expressing λN-HA or λN-HA-4EHP, GFP-MBP, and GFP-GIGYF1/2 (WT or GYF*). Two days post transfection, cells were treated with ActD and harvested at the indicated time points. *DBNDD2* mRNA levels were quantified by qRT-PCR and normalized to those of *18S* rRNA. Circles represent the mean value; error bars represent SD (n=3). The decay curves were fitted to an exponential decay with a single component (dotted lines). R^2 values are indicated for each curve.

Weber *et al.* Figure S2

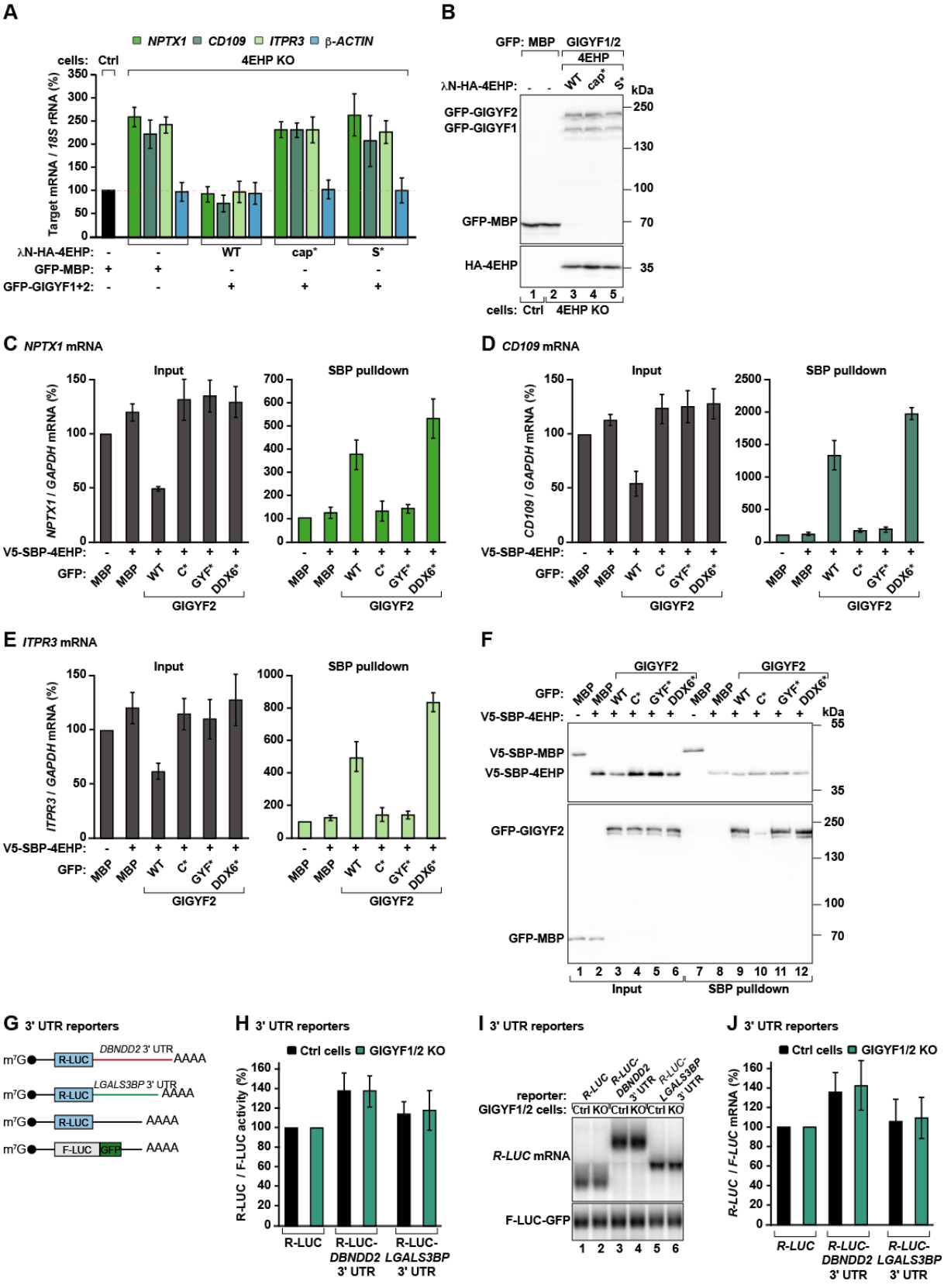

Figure S2, related to Figure 3. Binding of 4EHP to the cap and to GIGYF1/2 is crucial for mRNA decay.

(A) Control and 4EHP null cells were transfected with plasmids expressing λN-HA alone, wild type (WT) or the indicated λN-HA-4EHP mutants (cap-binding mutant: cap*, GIGYF1/2 specific-binding mutant: S*), GFP-

MBP or GFP-GIGYF1 and GFP-GIGYF2. *NPTX1*, *CD109*, *ITPR3* and *β-ACTIN* mRNA levels were determined by qRT-PCR and normalized to that of *18S* rRNA in the presence of the different 4EHP proteins. Bars represent the mean values and error bars denote the SD of three independent experiments.

(B) Western blot showing the expression levels of the proteins used in the experiments shown in (A). Blots were probed with anti-GFP and anti-HA antibodies.

(C-F) HEK293T cells were transfected with plasmids expressing V5-SBP-MBP or V5-SBP-4EHP, GFP-MBP or GFP-GIGYF2 (WT or mutants). Streptavidin binding protein-based pulldowns were performed two days post transfection and protein and RNA samples were collected for each experimental condition. *NPTX1*, *CD109* and *ITPR3* mRNA levels in input (0.8%) and IP samples (12%) were quantified by qRT-PCR, normalized over *GAPDH* and set to 100% in the presence of V5-SBP-MBP. Bars represent the mean value; error bars represent standard deviations from three independent experiments. (F) Western blot showing the expression of the proteins in the inputs (1% for the V5-SBP-tagged proteins and 0.5% for GFP-tagged proteins) and bound fractions (0.9% for the V5-SBP-tagged proteins and 2.7% for GFP-tagged proteins) from the experiments described in C-E.

(G) Schematic representation of the *DBNDD2* and *LGALS3BP* 3′ UTR reporters. *Renilla* luciferase (R-LUC); firefly luciferase (F-LUC); green fluorescent protein (GFP).

(H-J) Ctrl and GIGYF1/2 KO cells were transfected with the R-LUC-*DBNDD2*-3′ UTR, the R-LUC-*LGALS3BP*-3′ UTR or the R-LUC reporters and the transfection control F-LUC-GFP. (H) R-LUC activity was normalized to that of F-LUC-GFP and set to 100% for R-LUC in each cell line. (I) mRNA levels were determined by northern blotting. (J) *R-LUC*, *R-LUC-DBNDD2*-3′ UTR and *R-LUC-LGALS3BP*-3′ UTR band intensities were normalized to the intensity of *F-LUC-GFP* mRNA band and set to 100% for the R-LUC reporter in each cell line.

Weber *et al.* Figure S3

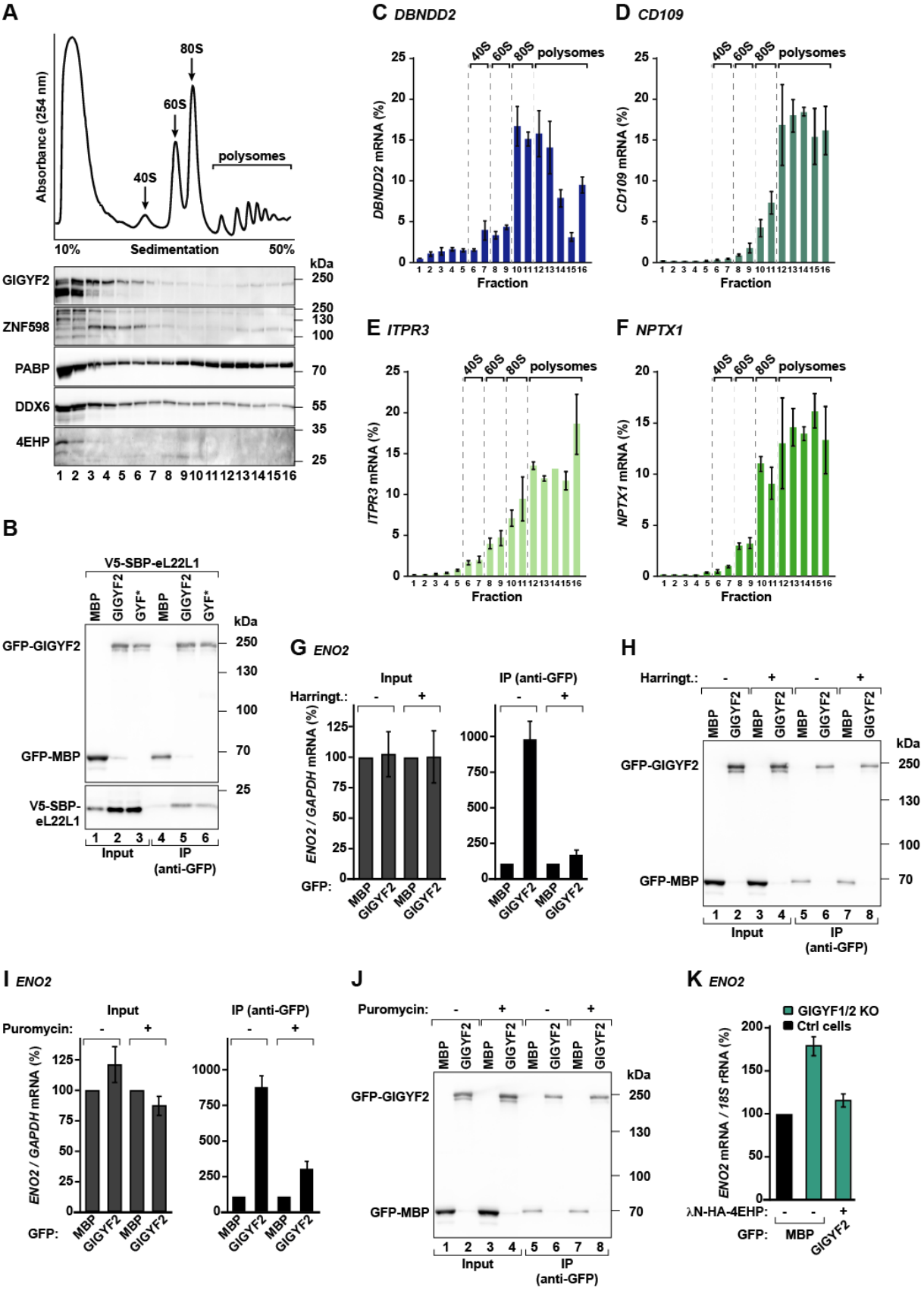

Figure S3, related to Figure 4. GIGYF1/2 promote decay of actively translating mRNAs

(A) UV absorbance profile at 254 nm of HEK293T cell extracts after polysome sedimentation in a sucrose gradient. 40S and 60S subunits, 80S monosomes, and polysome peaks are indicated. The distribution of GIGYF2, ZNF598, PABP, DDX6 and 4EHP across the gradient was analyzed by western blotting and is depicted below the profile.

(B) Immunoblot showing the interaction of GFP-GIGYF2 with V5-SBP-eL22L1 ribosomal protein. Proteins were immunoprecipitated using anti-GFP antibodies. GFP-MBP served as a negative control. The input (0.8% for the GFP proteins and 0.1% for V5-SBP-eL22L1) and immunoprecipitated fractions (12% for the GFP proteins and 24% for V5-SBP-eL22L1) were analyzed by western blotting with anti-GFP and anti-V5 antibodies.

(C-F) Abundance profiles for *DBNDD2*, *CD109*, *ITPR3* and *NPTX1* along the density gradient. mRNA levels were determined by qRT-PCR in samples prepared from total RNA extracted from each sucrose fraction. Bars represent the mean value; error bars denote the standard deviations from three independent experiments.

(G-J) HEK293T transfected with GFP-MBP or GFP-GIGYF2 were incubated with DMSO and the translational inhibitors harringtonine (G, H) or puromycin (I, J). After cell lysis, proteins were immunoprecipitated using anti-GFP antibodies. Protein and RNA samples were obtained for each experimental condition. Input (2%) and immunoprecipitated fractions (2.7%) were analyzed by western blotting. RNA samples were reversed transcribed and *ENO2* expression levels in input (0.8%) and IP samples (12%) were quantified by qRT-PCR, normalized to *GAPDH* and set to 100% in the presence of GFP-MBP. Bars represent the mean value and error bars the standard deviations from three independent experiments.

(K) Control and GIGYF1/2-null cells were transfected with plasmids expressing GFP-MBP or GFP-GIGYF2 and λN-HA-4EHP. RNA samples were collected and *ENO2* mRNA levels were quantified by qRT-PCR. mRNA levels were normalized to that of *18S* rRNA and set to 100% in Ctrl cells.

Weber *et al.* Figure S4

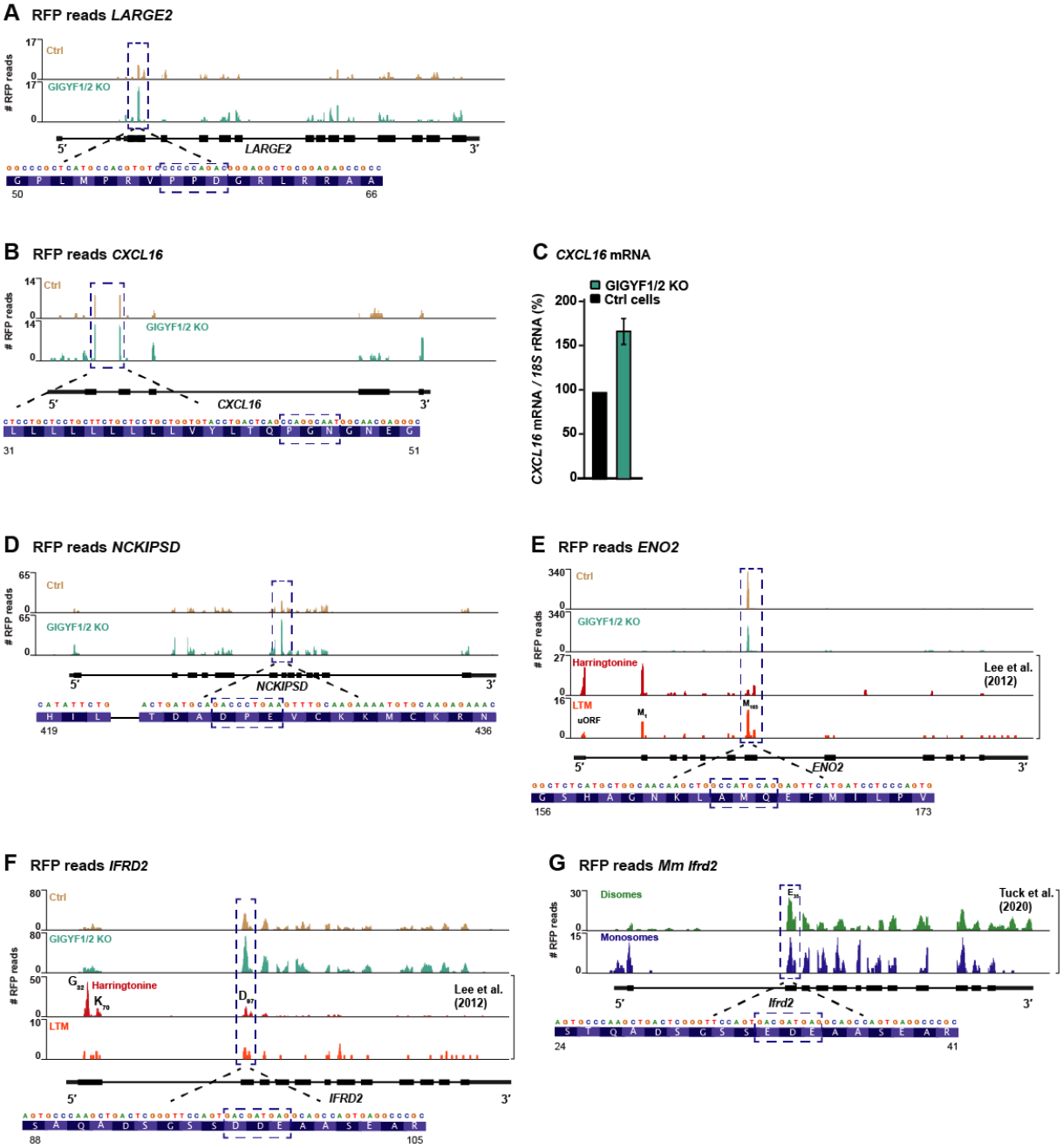

Figure S4, related to Figure 5. Ribosome density profiles in GIGYF1/2–4EHP target mRNAs reveal translational pausing

(A, B) Ribosome density profiles on *LARGE2* and *CXCL16*. The dashed blue box indicates the ribosome pause site. The nucleotide, peptide sequence at the pause site and residue numbering are depicted below the profiles.

(C) *CXCL16* mRNA steady state levels were quantified by qRT-PCR in control (Ctrl) and GIGYF1/2 null (KO) cells. mRNA levels were normalized to that of *18S* rRNA and set to 100% in Ctrl cells.

(D, E) Distribution of RFPs across the CDS of *NCKIPSD* and *ENO2* in Ctrl and GIGYF1/2 KO cells. Translational stalls with increased RFPs are highlighted with a dashed blue box. For *ENO2*, RFP distribution in

cells treated with the translational inhibitors harringtonine and lactimidomycin (LTM) obtained by Lee and co-workers (Lee et al., 2012) are also shown. Transcript organization, nucleotide and peptide sequence at the pause site, and residue numbering are depicted below the profiles. Upstream open reading frame (uORF), Met_1 (M_1), Met_{165} (M_{165}).

(F) RFPs distribution along the CDS of *IFRD2* in Ctrl, GIGYF1/2 KO, harringtonine- and LTM-treated cells (Lee et al., 2012). In cells treated with harringtonine, RFPs are observed at different positions of *IFRD2*; one of these corresponds to the paused ribosome at the DDE motif observed in this study. Transcript organization, nucleotide and peptide sequence at the pause site, and residue numbering are depicted below the profiles. Gly_{32} (G_{32}), Lys_{70} (K_{70}), Asp_{97} (D_{97}).

(G) Monosome and disome footprint distribution in *Mus musculus* (*Mm*) *Ifrd2*, as determined by Tuck and co-workers (Tuck et al., 2020). Of note is the occurrence of disomes at an equivalent position of the pause peptide observed in the human orthologue transcript. Transcript organization, nucleotide and peptide sequence at the pause site, and residue numbering are depicted below the profiles. Glu_{35} (E_{35}).

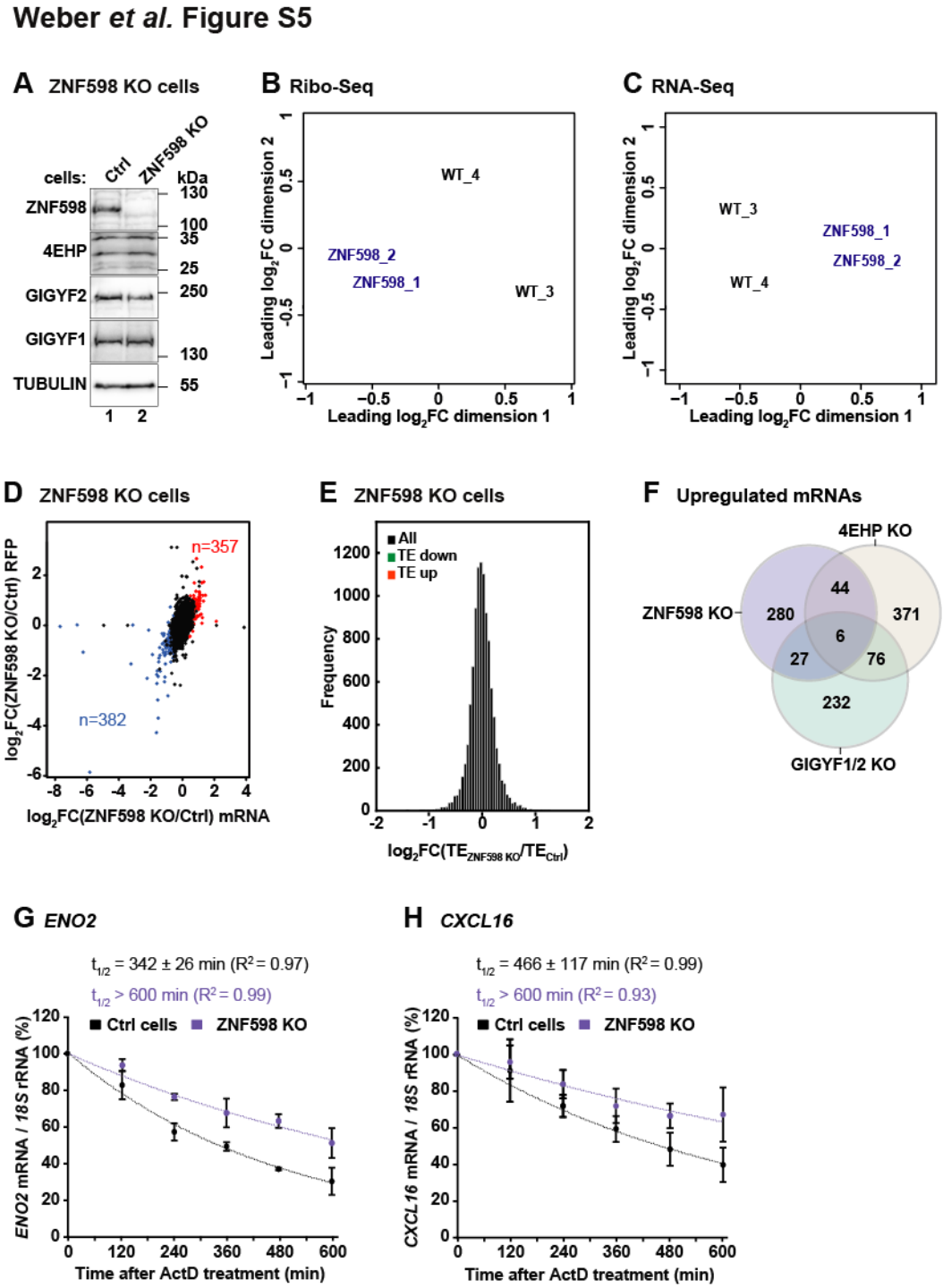

Figure S5, related to Figure 1. The ubiquitin ligase ZNF598 is only required for co-translational decay of a fraction of GIGYF1/2 targets

(A) Immunoblot showing the lack of ZNF598 expression in the null cells. 4EHP and GIGYF1/2 expression does not vary in ZNF598 null cells. TUBULIN was used as a loading control.

(B, C) Multidimensional scaling (MDS) analysis for the Ribo-Seq replicate libraries (B) and the RNA-Seq replicate libraries (C) from HEK293T WT and ZNF598 null cells.

(D) Genome-wide assessment of changes in RFPs and mRNA abundance in ZNF598 KO cells, depicted on a $\log_2$ scale. Each dot represents an individual gene (n_{total}=10453) with FPKM>2. In ZNF598 KO cells, 357 genes were significantly upregulated (FDR<0.005 and $\log_2$FC>0; red), whereas 382 genes were significantly downregulated (FDR<0.005 and $\log_2$FC<0; blue).

(E) Histogram showing the number of transcripts (frequency) in ZNF598 null cells with changes in TE ($\log_2$FC) relative to Ctrl cells. Transcripts with increased TE (n=5) in the absence of ZNF598 are shown in orange (FDR<0.005 and $\log_2$FC>0), whereas less translated transcripts (n=2) are depicted in green (FDR<0.005 and $\log_2$FC<0). See also Table S1.

(F) Venn diagram of the genes with increased mRNA abundance (upregulated genes) in ZNF598 null, GIGYF1/2 null and 4EHP null cells.

(G, H) Ctrl and ZNF598 KO HEK293T cells were treated with Actinomycin D (ActD) and harvested at the indicated time points. *ENO2* and *CXCL16* transcript levels were assessed by qRT-PCR and normalized to that of *18S* rRNA. The normalized value at time zero (before ActD addition) was defined as 100%. Results were plotted as a function of time post ActD addition. Circles represent the mean value; error bars represent the SD from three independent experiments. The decay curves were fitted to an exponential decay with a single component (dotted lines). R^2 values are indicated for each curve. The half-life of each mRNA in Ctrl (black) and null (purple) cells is represented as the mean +/- SD.

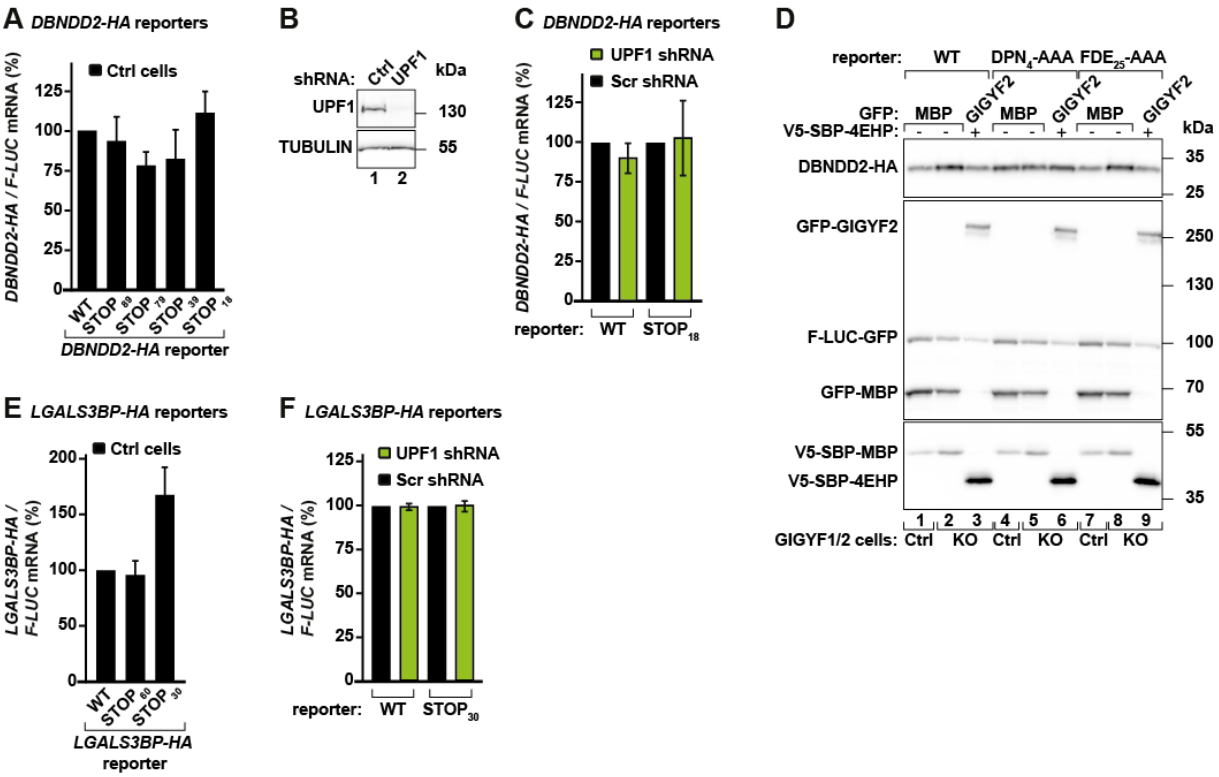

Figure S6, related to Figure 5. Wild type and mutant target-based CDS reporters

(A) Comparison of *DBNDD2-HA* (WT or $STOP_x$) reporter levels in HEK293T cells, as assessed by northern blotting (see Figure 5C). mRNA levels were normalized to *F-LUC-GFP* and set to 100% for the WT reporter. Bars represent the mean values and error bars denote the SD of three independent experiments.

(B) Western blot showing shRNA-mediated depletion of UPF1 in HEK293T cells. TUBULIN served as a loading control.

(C) HEK293T cells were treated with scramble (Scr) or shRNA targeting *UPF1* mRNA and transfected with *DBNDD2-HA* (WT or $STOP_{18}$) and *F-LUC-GFP*. The graph shows *DBNDD2-HA* mRNA abundance in control (Scr) and UPF1 KD cells. mRNA levels were determined by qRT-PCR, normalized to that of *F-LUC-GFP* and set to 100% in Scr-treated cells.

(D) Ctrl and GIGYF1/2-null cells were transfected with WT or mutant *DBNDD2-HA* plasmids. Protein samples were analyzed by western blotting using anti-V5, anti-HA and anti-GFP antibodies.

(E) Quantification of *LGALS3BP-HA* (WT or $STOP_x$) mRNA levels in HEK293T cells. RNA samples were analyzed by RT-qPCR (see Figure 6C). mRNA levels were normalized to *F-LUC-GFP* and set to 100% for the WT reporter. Bars represent the mean values and error bars denote the SD of three independent experiments.

(F) HEK2933T cells treated with Scr or UPF1 shRNAs were transfected with *LGALS3BP-HA* (WT or $STOP_{30}$) and *F-LUC-GFP*. *LGALS3BP-HA* mRNA levels were determined by RT-qPCR, normalized to that of *F-LUC-GFP* and set to 100% in Scr-treated cells.

Weber *et al.* Figure S7

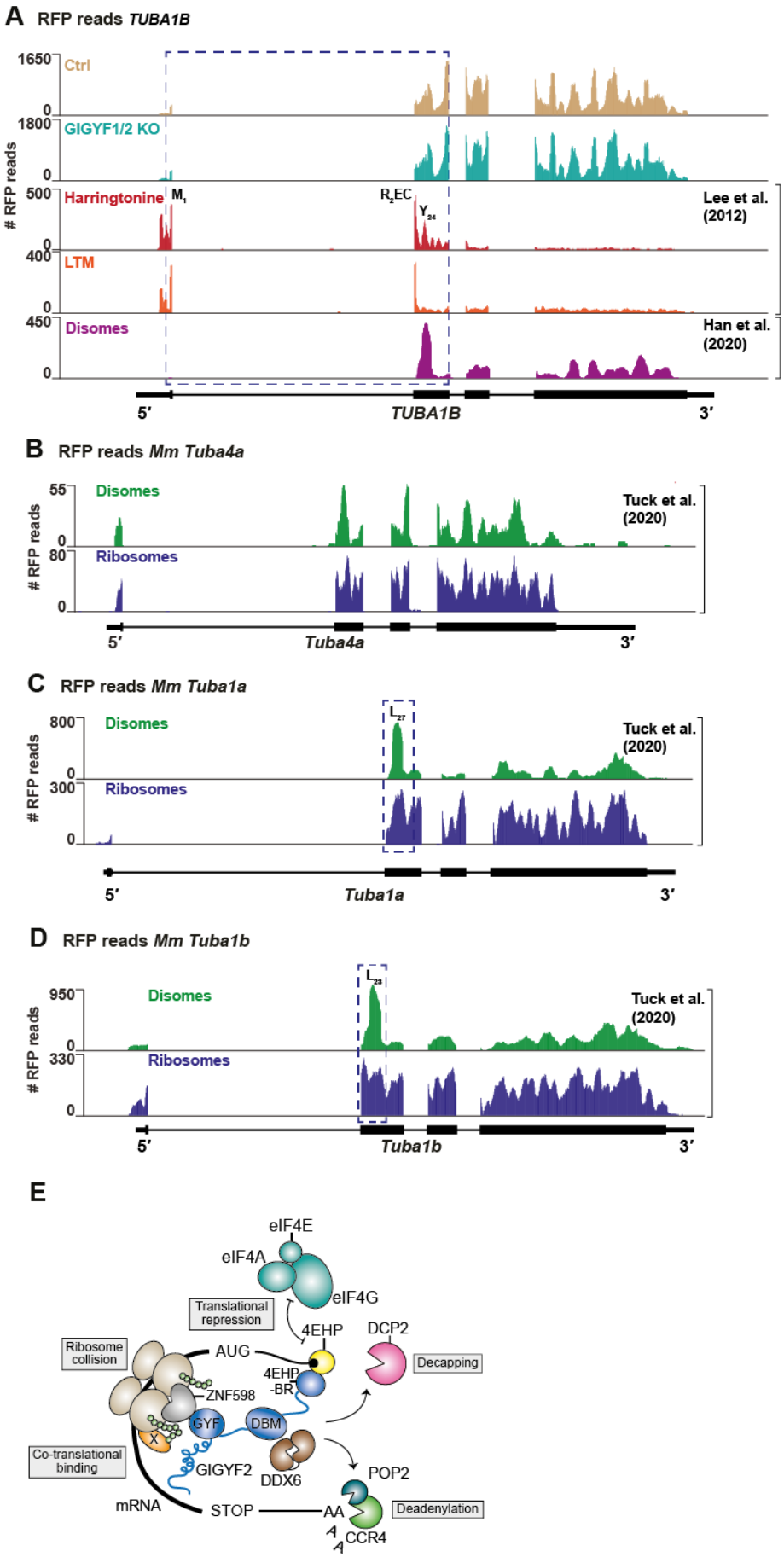

Figure S7, Related to Figure 7. Monosome and disome density profiles in *TUBULIN* mRNAs reveal translational pausing

(A) RFP of *TUBA1B* in Ctrl, GIGYF1/2 KO, and cells treated with harringtonine or lactimidomycin (LTM) as determined by Lee and co-workers (Lee et al., 2012). Harringtonine footprints identify the initiating ribosome at the translation start site (M_1) and paused elongating ribosomes (dashed blue square). The profile also shows the distribution of disome footprints along the CDS in HEK293 cells as obtained by Han and co-workers (Han et al., 2020). Met_1 (M_1); Arg_2 (R_2), Glu (E), Cys (C), Tyr_{24} (Y_{24}). Transcript UTRs, intron and exons are depicted below the profiles.

(B-D) Monosome and disome density profiles of *Mm Tuba1a*, *Tuba4a* and *Tuba1b* transcripts based on the data previously obtained by Tuck and co-workers in mouse embryonic stem cells (Tuck et al., 2020). The dashed blue box indicates the occurrence of ribosome collision (disomes) in the first 20-30 codons of tubulins. Transcript UTRs, intron and exons are depicted below the profiles.

(E) Recruitment of 4EHP-GIGYF1/2 complexes to transcripts with perturbed elongation induces translation repression, mRNA deadenylation and decapping. 4EHP, in yellow, competes with eIF4F (eIF4E+eIF4G+eIF4A) for cap-binding, blocking translation and promoting decapping. Binding of 4EHP to the mRNA depends on GIGYF1/2 proteins (in blue), the scaffolds of the repressor complexes. mRNA selection involves the recognition of paused ribosomes by factors such as the E3 ubiquitin ligase ZNF598 (in grey), which binds to the GYF domain of GIGYF1/2. In addition, target selection can be favored by co-translational binding of components of the surveillance machinery (X) to the nascent peptide chain. Recognition of the nascent chain by specific factors (X), or the synthesis of the nascent peptide itself, might then interfere with ribosome activity, causing ribosome pausing and collisions. Detection of such events coupled to the recruitment of 4EHP and GIGYF1/2, exposes the translating mRNA to degradation. GIGYF1/2 also recruit the RNA helicase DDX6 which is required for target repression and decay. Altogether, GIGYF1/2 initiate a series of events that irrevocably prevent the translation of mRNAs with impaired elongation. DCP2: decapping enzyme 2; POP2 and CCR4: deadenylases; 4EHP-BR: 4EHP-binding region; DBM: DDX6-binding motif.

Table S6. Genes commonly upregulated in ZNF98 null, GIGYF1/2 null and 4EHP null HEK293T cells. Related to Figure 1.

ZNF598 null and GIGYF1/2 null cells	ZNF598 null and 4EHP null cells
Gene name	**Gene name**
ABCA3	AACS
AIFM2	ALG1L
AMIGO1	APOBEC3B
APOL2	APOE
BASP1	ARHGEF2
BEX5	ARHGEF6
CCDC88C	ARMCX5-GPRASP2
CHRDL1	ATF3
COL1A1	CLU
CXCL16	CSTF2T
CYP2J2	CXCL16
EHD2	CYR61
ENO2	DDR2
HLA-DPA1	DIAPH3
IFI6	DNMT1
IFIH1	EEF1A2
IFIT5	EIF2AK2
IFITM1	EMP3
KIF1A	ENO2
KRT18	FLNA
MGST1	FLNC
MLLT11	GPRASP2
NDRG1	HLA-DPA1
NELL2	IFITM2
NQO1	JUN
PLEKHG4	KHK
PSMB9	KIF1A
RHOB	KLF10
TCEAL3	LPIN1
TP53I3	MAP1B
TRIB1	MED12
TRIM47	MRC2
UBE2L6	MSH2
	OPTN
	PDE7A
	PDP1
	PLEKHA2
	PLEKHG4
	PLEKHH3
	PTRF
	RAB3GAP2
	RAB6B
	RNF213
	SLAIN1
	TBC1D32
	TCEAL3
	TNFRSF12A
	TRIM25
	TTLL7
	TUBB4A

Table S7. primers used in this study. Related to STAR Methods.

		sequence (5' to 3')
qPCR		
DBNDD2	fwd	CCAGCAGCTCCGCCTTC
	rev	GTTGTCCACCCCAGACGAC
CD109	fwd	GGTTGAGGAGCATACTGAAAAT
	rev	TGGCAGTCTAATGCTCACACCC
NPTX1	fwd	TCTGCAGGGATCTTCTCCGTTT
	rev	TCCCAGCTGTGGGAATCCTTTA
ITPR3	fwd	CTGCTGCATTTGTGGACACCTG
	rev	CACTACGCAGGTCAGCGAAGGT
ENO2	fwd	ATGTGTCACTTGTGCTTTGCTC
	rev	ACCCCAGTCATCTTGGGATCTA
CXCL16	fwd	CTCCAGATCTGCCGGTTCATTA
	rev	ATCACCCAGTGTGAAAAGCAGA
TUBA4A	fwd	TGAAACTGGTGCTGGAAAACAC
	rev	CTCCATCAGGAGTGAGGTGAAG
TUBB4A	fwd	CTCGAGGCTTCTGACCTTTGAT
	rev	TTAAAGGTGCGGTTTCCAGAGT
TUBA1A	fwd	CCACAGTCATTGATGAAGTTCG
	rev	GCTGTGGAAAACCAAGAAGC
TUBA1B	fwd	AATTCGCAAGCTGGCTGA
	rev	CGACAGATGTCATAGATGGCC
TUBB	fwd	GAAGCCACAGGTGGCAAATA
	rev	CGTACCACATCCAGGACAGA
GAPDH	fwd	CTCTGCTCCTCCTGTTCGACAG
	rev	TTCCCGTTCTCAGCCTTGACGG
β-ACTIN	fwd	GCAGGAGTATGACGAGTCCGGC
	rev	GTAACAACGCATCTCATATTTG
18S rRNA	fwd	CAGCCACCCGAGATTGAGCA
	rev	TAGTAGCGACGGGCGGTGTG
LGALS3BP-HA	fwd	CTGGGCCTCACCAAGTCTGGCG
	rev	AGCGTAATCTGGAACATCGTAT
DBNDD2-HA	fwd	CCAGCAGCTCCGCCTTC
	rev	AGCGTAATCTGGAACATCGTAT
sgRNA		
sg4EHP-a	TATAGCCACATGGTACGTCC	
sg4EHP-b	TGTTTTCTTCATTCTGATCA	
sgZNF598	CTACTGCGCCGTGTGCCGCG (Garzia et al., 2017)	
sgZNF598	GAAAGGTGTACGCATTGTAC (Garzia et al., 2017)	
shRNA		
Scramble	ATTCTCCGAACGTGTCACG (Jonas et al., 2013)	
UPF1-I	GAGAATCGCCTACTTCACT (Paillusson et al., 2005)	
UPF1-II	GATGCAGTTCCGCTCCATT (Paillusson et al., 2005)	
Ribosome profiling		

30 nt RNA marker	AUGUACACGGAGUCGAGCUCAACCCGCAAC-P
27 nt RNA marker	AUGUACACGGAGUCGAGCUCAACCCGC-P
3' adapter	rApp/NNNNT GGA ATT CTC GGG TGC CAA GG/3InvdT/
5' adapter (RNA)	GUUCAGAGUUCUACAGUCCGACGAUCNNNN
Reverse transcription primer	GCCTTGGCACCCGAGAATTCCA
Forward primer	AATGATACGGCGACCACCGAGATCTACACGTTCAGAGTT CTACAGTCCGA
Barcoded reverse primer	CAAGCAGAAGACGGCATACGAGATNNNNNNGTGACTGG AGTTCCTTGGCACCCGAGAATTCCA